RECORD #
AAA0003
AAB3/81

RM No. L7I10

AERONAUTICS LIBRARY
California Institute of Technology

NACA

RESEARCH MEMORANDUM

HYDRODYNAMIC CHARACTERISTICS OF A LOW-DRAG, PLANING-TAIL FLYING-BOAT HULL

By

Henry B. Suydam

Langley Aeronautical Laboratory
Langley Field, Va.

CLASSIFIED DOCUMENT

This document contains classified information affecting the National Defense of the United States within the meaning of the Espionage Act, USC 50:31 and 32. Its transmission or the revelation of its contents in any manner to an unauthorized person is prohibited by law. Information so classified may be imparted only to persons in the military and naval services of the United States, appropriate civilian officers and employees of the Federal Government who have a legitimate interest therein, and to United States citizens of known loyalty and discretion who of necessity must be informed thereof.

NATIONAL ADVISORY COMMITTEE
FOR AERONAUTICS

WASHINGTON
October 21, 1948

CLASSIFICATION cancelled

NATIONAL ADVISORY COMMITTEE FOR AERONAUTICS

RESEARCH MEMORANDUM

HYDRODYNAMIC CHARACTERISTICS OF A LOW-DRAG, PLANING-TAIL FLYING-BOAT HULL

By Henry B. Suydam

SUMMARY

The hydrodynamic characteristics of a flying-boat incorporating a low-drag, planing-tail hull were determined from model tests made in Langley tank no. 2 and compared with tests of the same flying boat incorporating a conventional-type hull. The planing-tail model, with which stable take-offs were possible for a large range of elevator positions at all center-of-gravity locations tested, had more take-off stability than the conventional model. No upper-limit porpoising was encountered by the planing-tail model. The maximum changes in rise during landings were lower for the planing-tail model than for the conventional model at most contact trims, an indication of improved landing stability for the planing-tail model. The hydrodynamic resistance of the planing-tail hull was lower than the conventional hull at all speeds, and the load-resistance ratio was higher for the planing-tail hull, being especially high at the hump. The static trim of the planing-tail hull was much higher than the conventional hull, but the variation of trim with speed during take-off was smaller.

INTRODUCTION

In the search for a flying-boat hull that would have low air drag, wind-tunnel tests were run on several models of planing-tail-type flying-boat hulls. The results of these tests are given in references 1 and 2 and indicate that a deep-stepped planing-tail hull with a very full step fairing will have low air drag, much lower than a comparable conventional-type hull. Resistance tests previously run on planing-tail-type hulls (references 3, 4, and 5) indicate

CLASSIFICATION cancelled

that this type hull can be expected to have lower hydrodynamic resistance than a comparable conventional-type hull. To evaluate the hydrodynamic characteristics of this low-drag, planing-tail hull, a model of a large contemporary flying boat was fitted with a planing-tail hull whose lines were similar to those of the lowest-drag hull reported in reference 2. The results of hydrodynamic tests of this model conducted in Langley tank no. 2 are given in the present report and compared with results of previous tests of the same model with the conventional-type hull. The procedure of reference 6 was used to evaluate the major hydrodynamic qualities.

COEFFICIENTS AND SYMBOLS

The speed, resistance, and load on the model were reduced to the following nondimensional coefficients based on Froude's criterion for similitude:

C_V speed coefficient $\left(\frac{V}{\sqrt{gb}}\right)$

C_R resistance coefficient $\left(\frac{R}{wb^3}\right)$

C_Δ load coefficient $\left(\frac{\Delta}{wb^3}\right)$

V speed, feet per second

g acceleration of gravity, feet per second per second

b maximum beam of hulls (1.125 ft)

R resistance, pounds

w specific weight of water (63.5 lb/cu ft in these tests)

Δ load on water, pounds

Trim angle between forebody keel and horizontal

M.A.C. mean aerodynamic chord

MODEL AND APPARATUS

To gain an evaluation of the hydrodynamic characteristics of the low-drag, planing-tail hull in the shortest possible time, an existing dynamic model was modified to obtain a hull form as similar as possible to the hull of reference 2 which had the lowest air drag of any tested in that series. The resulting hull differed in some respects from the one tested in the wind tunnel, due to limitations imposed by fitting it to the existing model. The sternpost angle was held the same for the tank model as for the wind-tunnel model, but the length-beam ratio and the depth of step were lower for the tank model. It is realized that the aerodynamic characteristics of this tank model will probably differ to some extent from those of the wind-tunnel model. However, the extreme step fairing, which is the feature most suspect of adversely affecting hydrodynamic performance, has been made fuller on the tank model than on the wind-tunnel model. Any hydrodynamic difficulty chargeable to the fairing would thus be accented by the tank model.

A photograph of the modified dynamic model with the planing-tail hull is shown in figure 1, and the general arrangement and hull lines are given in figures 2 and 3, respectively. To facilitate a direct comparison of the hydrodynamic characteristics of the planing-tail hull and the conventional-type hull, results are given for a series of tests of the dynamic model of the same contemporary flying boat which was used as a parent airplane for the planing-tail modification. The general arrangement and body plan of this model are shown in figures 4 and 5, respectively. The maximum beam was held the same and the gross weight, moment of inertia, and static propeller thrust were held as nearly the same as possible for the planing-tail configuration as for the conventional-hull model.

The aerodynamic surfaces of the two models were the same, but their locations on the models were slightly different, as shown in the list of principal dimensions for the two models. (See table I.) The horizontal tail moment arm of the planing-tail configuration was inadvertently made 1.85 inches shorter than the conventional-hull configuration, and the dihedral was deliberately eliminated to facilitate model construction. However, the stabilizer was adjusted to give the same pitching moment at 0° trim as the conventional-hull configuration. The angle of incidence of the wing of the planing-tail configuration was held the same with respect to the deck line as the conventional model, but the tangent to the forebody keel at the step for the planing-tail configuration was made to coincide with the base

line, instead of forming a 2° angle with the base line, as was the case for the contemporary flying boat. Since the trim angle for both models was measured as the angle formed between a line tangent to the forebody keel at the step and the water surface, the planing-tail model would have a 2° higher angle of attack of the wing than the conventional-hull model for the same trim angle. This would have very little effect on the stability characteristics of the models, since both models would still operate on the straight portion of the lift curve below the stall at the highest trims tested; but it would have some effect on the resistance, due to the change in the load on the water for the two models at the same trim and speed.

The dynamic planing-tail model was constructed of balsa and tissue in the conventional manner and was powered by electrically driven adjustable-pitch propellers. Gross load coefficient of the model was 0.94 and, with the center of gravity located at 28 percent of the mean aerodynamic chord, the value of the moment of inertia was approximately 8.4 slug-feet^2. For the stability tests, the model was attached to the towing carriage free to pitch and free to rise. Control of the model was by means of the elevators, which were controllable through a range of ±30° deflection.

TEST PROCEDURES

Center-of-Gravity Limits of Stability

The center-of-gravity limits of stability of the model were found by the usual method of making an accelerated run to get-away, with fixed elevators, holding a constant acceleration of 1 foot per second per second. Full power was used on all runs, and the model trim, rise, and amplitude of porpoising were recorded on wax-coated paper by a pointer attached to the model. A sufficient number of center-of-gravity locations and elevator deflections were tested to cover the normal range of values and to define closely the stability limits. The variation of trim with speed for the various conditions was also observed during these runs.

Trim Limits of Stability

The standard technique employed in the NACA tanks was used to ascertain the trim limits of stability. The towing carriage was held at constant speed, while the model trim was slowly increased

or decreased with the elevators until the porpoising limit was crossed. The lower limit and the upper limit, increasing trim, were considered to be the trims where porpoising oscillations started; and the upper limit, decreasing trim, is defined as the trim assumed by the model at the instant upper-limit porpoising ceases. Where no upper trim limit of stability curves appeared, no upper-limit porpoising was encountered by the model.

Landing Stability

The landing stability of the model was investigated by trimming the model in the air to the desired landing trim while the carriage was held at a constant speed slightly above model flying speed and then decelerating the carriage at the uniform rate of 3 feet per second per second, allowing the model to glide onto the water and to simulate an actual landing as the speed fell below flying speed. The model was restrained from rising more than 2 inches clear of the water to hold the sinking speed to reasonable values. The landing trims and model behavior were observed visually, and records of the angular and vertical displacement of the model during the landings were scribed on sheets of wax-coated paper. Landings generally were made with the motors set to deliver approximately one-quarter of the full power used during take-off runs.

Resistance

As the resistance of the conventional-hull model was not found in the previous tests, the resistance of this model was determined by separate tests run in Langley tank no. 2 to facilitate a direct comparison of the resistance characteristics of the low-drag planing-tail model and the conventional-hull model. The hulls of the two dynamic models were tested under similar conditions with wing and tail removed, using the standard resistance dynamometer. The models were tested fixed in trim and at constant speeds. The range of trims tested at any speed was determined from the hydrodynamic stability tests as being the range of stable trims attainable at that speed by the use of the elevators alone. The load on the water at a given trim and speed was determined from the aerodynamic lift curves of the contemporary flying boat. The same initial gross load coefficient of 0.94 was used for both models, and the center of gravity was considered to be located at 30 percent M.A.C. The resistance selected at each speed for comparison was the lowest resistance obtained at that speed.

RESULTS AND DISCUSSION

Take-Off Stability

The take-off stability is given for the two configurations in figure 6 as a plot of elevator position against center-of-gravity location. For the conventional-hull model, there is a range of center-of-gravity positions from 27 percent M.A.C. to about 46 percent M.A.C., for which stable take-offs are possible. The range of elevator deflections for stable take-offs increases rapidly from about 5° at 27 percent M.A.C. to 13° at 30 percent M.A.C. and remains approximately constant at 13° for the range of center-of-gravity positions from 30 percent M.A.C. to 36 percent M.A.C. Aft of 36 percent M.A.C., the range of negative elevator positions available decreases rapidly to about 5° at 42 percent M.A.C., but this decrease is probably compensated for by an increase in available positive elevator positions. No tests were made with positive elevator deflections. For the planing-tail configuration, stable take-offs were possible at all center-of-gravity locations tested from 22 percent M.A.C. to 41 percent M.A.C. At 22 percent M.A.C., the range of elevator deflections available for stable take-offs was about 12°; and this range increased continuously to a full 30° at 41 percent M.A.C. Thus for all center-of-gravity positions, stable take-offs are possible with the planing-tail configuration at elevator deflections of -18° and greater.

The trim limits of stability for the two configurations (fig. 7) offer an explanation for the very good take-off stability of the planing-tail model. The conventional-hull model first encountered the lower porpoising limit at a speed coefficient of about 3, which is just beyond the hump speed for the model, and at a trim of about $7\frac{1}{2}°$. It encountered the upper trim limit first at a speed coefficient of 4.2 and at a trim of about 10°. The stable range between these limits is restricted, and if the elevator deflection and center-of-gravity location are adjusted to avoid the lower porpoising limit, there is a relatively small range of higher elevator deflections or more aft positions of the center of gravity available for stable take-offs before the upper porpoising limit will be crossed. For the planing-tail model, however, the lower porpoising limit was not encountered until a speed coefficient of about 4.2 was reached with a corresponding trim of 3°; and no upper porpoising limit was encountered at any trim or speed. The maximum trim attainable with full elevator deflection is shown in figure 7. Conceivably, an

upper porpoising limit does exist for this model at trims above this maximum attainable trim. This combination, or lack, of porpoising limits gives a very large stable range and makes available for stable take-offs a much greater combination of elevator deflections and center-of-gravity positions for the planing-tail configuration than for the conventional-hull model.

Landing Stability

During a landing a flying boat experiences a series of rise changes or heaves which may be insignificant or may be large enough to cause the airplane to leave the water, a behavior that is commonly known as skipping. The greatest of these rise changes experienced during a landing is designated the maximum change in rise. Values of this maximum change in rise for the planing-tail model were obtained during landings at various contact trims throughout the normal operating trim range. These maximum changes in rise are plotted against contact trim in figure 8, and this curve is compared with the curve of landing stability for the conventional-hull model, taken from figure 6 of reference 6. The conventional-hull model has a narrow range of bad landing stability at contact trims from 6° to 7° with a severe discontinuity at a contact trim of 7°. Below 6° and above 7° landings are generally acceptable. In contrast, the curve of landing stability for the planing-tail model is smooth and continuous at all contact trims, and is well below the maximum rise for the conventional-hull model over most of the trim range. This performance for the planing-tail model is somewhat unexpected in view of the very full step fairing with which the model was fitted. Past experience has indicated that extreme step fairings have a tendency to cause landing instability, necessitating either removal or retraction of the fairing. Figure 8, however, indicates that the very deep, pointed step of the planing-tail hull can be fitted with an extreme aerodynamic step fairing and still maintain good landing stability.

Resistance

The hydrodynamic resistance curves of the planing-tail and conventional-hull models are given in figure 9. Here the resistance is seen to be lower for the planing-tail hull than for the conventional hull; it is considerably lower throughout the major portion of the curve at hump speed and beyond through intermediate and high speeds. Because of the difference in the angle between the wing chord line and the keel for the two models, however, this considerably lower resistance for the planing-tail hull cannot all be attributed to the more efficient hull form.

The curves of trim against speed coefficient which were used to obtain the resistance curves of figure 9 are given in figure 10 for the two models. The curves of load coefficient against speed coefficient for the two models which correspond to the trim curves are also shown in figure 10. For any given speed of the model, the trim and load coefficient found in figure 10 were applied to the model to obtain the resistance coefficient given in figure 9. At rest, both models have a load coefficient of 0.94 without power, but as the load curves are derived from the aerodynamic lift curves using full power, the static load coefficient is considerably lower for the planing tail than for the conventional-hull model. This decrease is due partly to the 2° higher angle of incidence of the wing on the planing-tail model, but is mainly due to the much higher trim and consequently higher angle of attack of the planing-tail model, which is a definite advantage attributable directly to the planing-tail-type hull. The load coefficient is lower for the planing-tail hull than for the conventional hull at all speeds for the same reasons - that is, 2° higher angle of incidence and generally higher trim for the planing-tail model.

To eliminate the effect of the different load coefficients of the two models and to obtain a direct comparison of hull efficiencies, a plot of load-resistance ratio against speed coefficient is given in figure 11. The planing-tail hull has a much higher efficiency at the hump than the conventional hull, with a load-resistance ratio of 6.2 as compared with 4.8 for the conventional hull. Comparison of the load-resistance ratios for the planing-tail hull at high speeds with results of reference 4 indicates that present values are normal for the planing-tail hull type. The load-resistance ratios for the conventional hull, however, are somewhat surprising, being higher in the high-speed region than values generally obtained for conventional-type hulls.

Variation of Trim with Speed

The variations of trim with speed during take-off, shown for the planing-tail model in figure 12 and for the contemporary model in figure 13, illustrate the fundamentally different take-off characteristics of the two hulls. In figure 12, curves are given for elevator deflections of 0° and -30° while in figure 13, elevator deflections of -5° and -25° are used. The smaller range of elevator positions tested on the conventional-hull model was necessary to avoid very severe porpoising.

At rest, the contemporary model has a trim of slightly less than 1°. As speed is increased, the trim first drops slightly and then increases rapidly to a peak at a speed coefficient of about 3, after which it falls off rapidly to a speed coefficient of about 4. The planing-tail model has a trim at rest of slightly less than 6°, much higher than the contemporary model; but as speed is increased, the model increases trim gradually until it reaches a speed coefficient of about 4. Above a speed coefficient of 4, the elevators of both models become very effective, and a large range of trims is attainable by each model.

Typical curves of variation of trim with speed during a take-off are those given in figure 10. The total trim variation for the conventional-hull model here is about $7\frac{1}{2}^{\circ}$ while the variation for the planing-tail model for the entire take-off run is only about 2°. This smaller variation of trim with speed for the planing-tail model is explained by the very deep step, which accounts for the high trim at rest, and the long afterbody, which prevents the model from trimming up very high during the early part of the take-off run. At high speeds the elevators are very effective, and the trim is determined primarily by the elevator position, as is the case for the conventional model.

Spray Characteristics

No detailed investigation was made of the spray characteristics of the planing-tail model. However, as the forebody of the planing-tail model had the same maximum beam and only slightly greater length than the forebody of the conventional-hull model, while both models had the same gross load, no noticeable difference in spray entering the propellers or striking the flaps was expected. Visual observation indicated that the spray entering the propellers and the spray impinging on the flaps were approximately the same for the planing-tail model as those for the conventional-hull model. The horizontal tail surfaces were moderately wetted by spray at speed coefficients from about 3 to about 5, and this wetting was less severe with full power than without power. Raising the horizontal tail slightly and incorporating dihedral should be sufficient to eliminate spray over these tail surfaces.

CONCLUSIONS

The results of model tests to determine the hydrodynamic characteristics of a low-drag, planing-tail, flying-boat hull indicate that generally favorable conclusions may be drawn relative to the performance of this hull as compared with the performance of a conventional-type hull. The planing-tail model had a large range of elevator positions available for stable take-offs at all center-of-gravity locations tested, from 22 percent M.A.C. to 41 percent M.A.C., while stable take-offs were not possible with the conventional model forward of 27 percent M.A.C. No upper-limit porpoising was encountered by the planing-tail model at any time. The planing-tail model encountered no skipping or severe landing instability at any contact trim, and the maximum changes in rise during landings were lower than those for the conventional model at all contact trims above $5\frac{1}{2}^{\circ}$. The hydrodynamic resistance of the planing-tail hull was lower than the resistance of the conventional hull at all speeds, and the load-resistance ratio was higher for the planing-tail hull than for the conventional hull, especially at the hump where the planing-tail hull had a value of 6.2 as compared with 4.8 for the conventional hull. The trim of the planing-tail model at rest was 6°, compared with a trim of about 1° for the conventional model. The variation of trim with speed during take-off was generally much smaller for the planing-tail model than for the conventional model.

Langley Aeronautical Laboratory
National Advisory Committee for Aeronautics
Langley Field, Va.

REFERENCES

1. Yates, Campbell C., and Riebe, John M.: Aerodynamic Characteristics of Three Planing-Tail Flying-Boat Hulls. NACA TN No. 1306, 1947.

2. Riebe, John M., and Naeseth, Rodger L.: Aerodynamic Characteristics of Three Deep-Step Planing-Tail Flying-Boat Hulls. NACA RM No. L8I27, 1947.

3. Dawson, John R., and Wadlin, Kenneth L.: Preliminary Tank Tests with Planing-Tail Seaplane Hulls. NACA ARR No. 3F15, 1943.

4. Dawson, John R., Walter, Robert C., and Hay, Elizabeth S.: Tank Tests to Determine the Effect of Varying Design Parameters of Planing-Tail Hulls. I - Effect of Varying Length, Width, and Plan-Form Taper of Afterbody. NACA TN No. 1062, 1946.

5. Dawson, John R., McKann. Robert, and Hay, Elizabeth S.: Tank Tests to Determine the Effect of Varying Design Parameters of Planing-Tail Hulls. II - Effect of Varying Depth of Step, Angle of Afterbody Keel, Length of Afterbody Chine, and Gross Load. NACA TN No. 1101, 1946.

6. Parkinson, John B.: Appreciation and Determination of the Hydrodynamic Qualities of Seaplanes. NACA TN No. 1290, 1947.

TABLE I

	Planing-tail model	Conventional-hull model
Hull:		
Beam, maximum, in.	13.50	13.50
Length of forebody, in.	52.00	48.16
Length of afterbody, in.	72.00	41.87
Length of tail extension, in.	0	30.29
Length over all, in.	124.00	120.32
Depth of unfaired step, in.	6.07	0.63
Angle of forebody keel, deg	0	2.0
Angle of afterbody keel, deg	5.3	5.0
Angle of deadrise, main planing bottom, deg	20.0	20.0
Wing:		
Area, sq ft	25.58	25.58
Span, in.	200.00	200.00
Mean aerodynamic chord, M.A.C., in.	20.12	20.12
Leading edge M.A.C		
Aft of bow, in.	43.39	37.98
Above base line, in.	20.48	20.22
Angle of wing setting to base line, deg	5.5	5.5
Angle of wing setting to forebody keel, deg	5.5	3.5
Horizontal Tail Surfaces:		
Span, in.	61.67	61.67
Area, stabilizer, sq ft	3.04	3.04
Area, elevator, sq ft	2.77	2.77
Angle of stabilizer to base line, deg	0	3.0
Dihedral, deg	0	8.0
Leading edge of stabilizer		
Aft of bow, in.	105.76	102.20
Above base line, in.	24.00	25.00

NATIONAL ADVISORY
COMMITTEE FOR AERONAUTICS



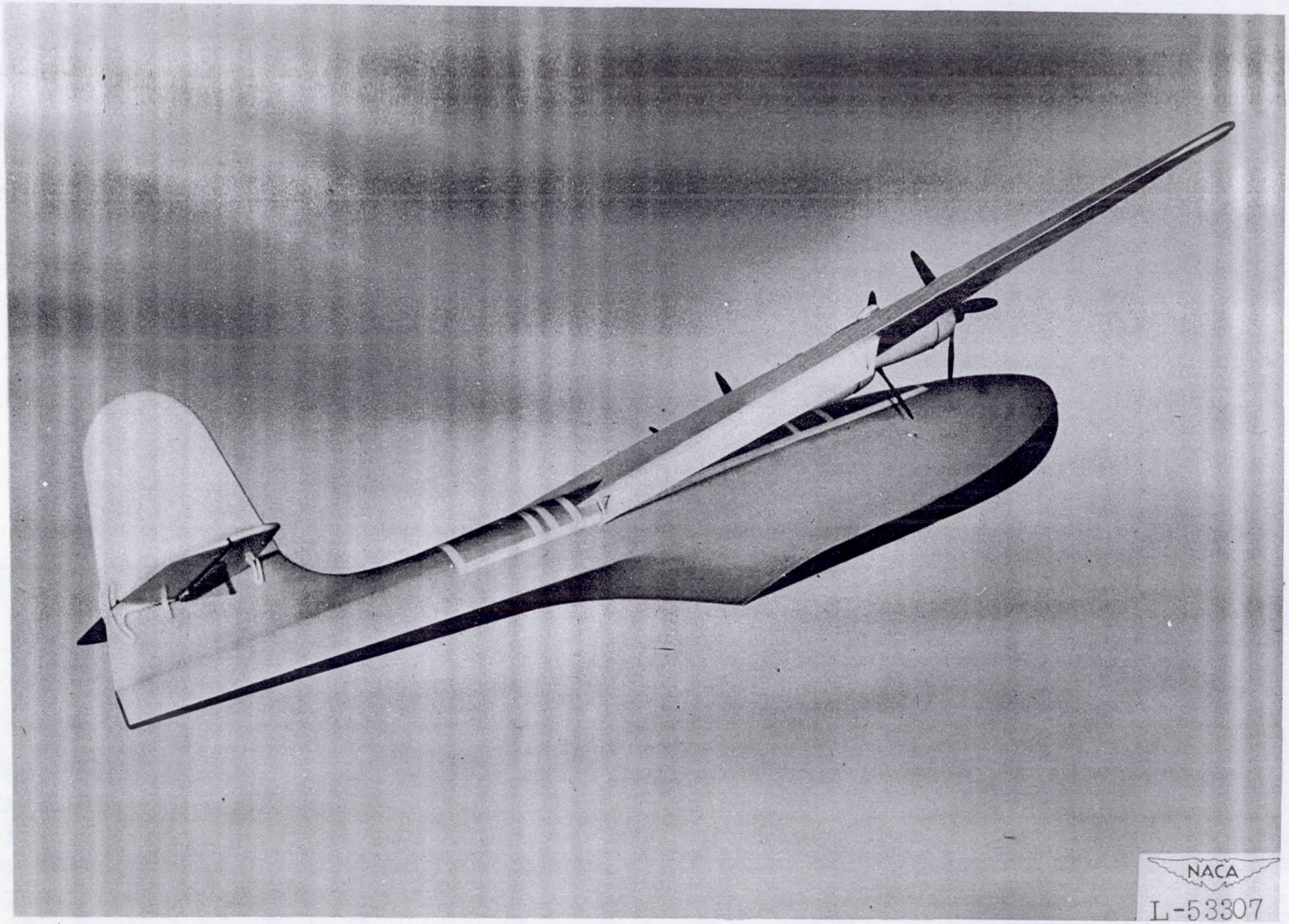
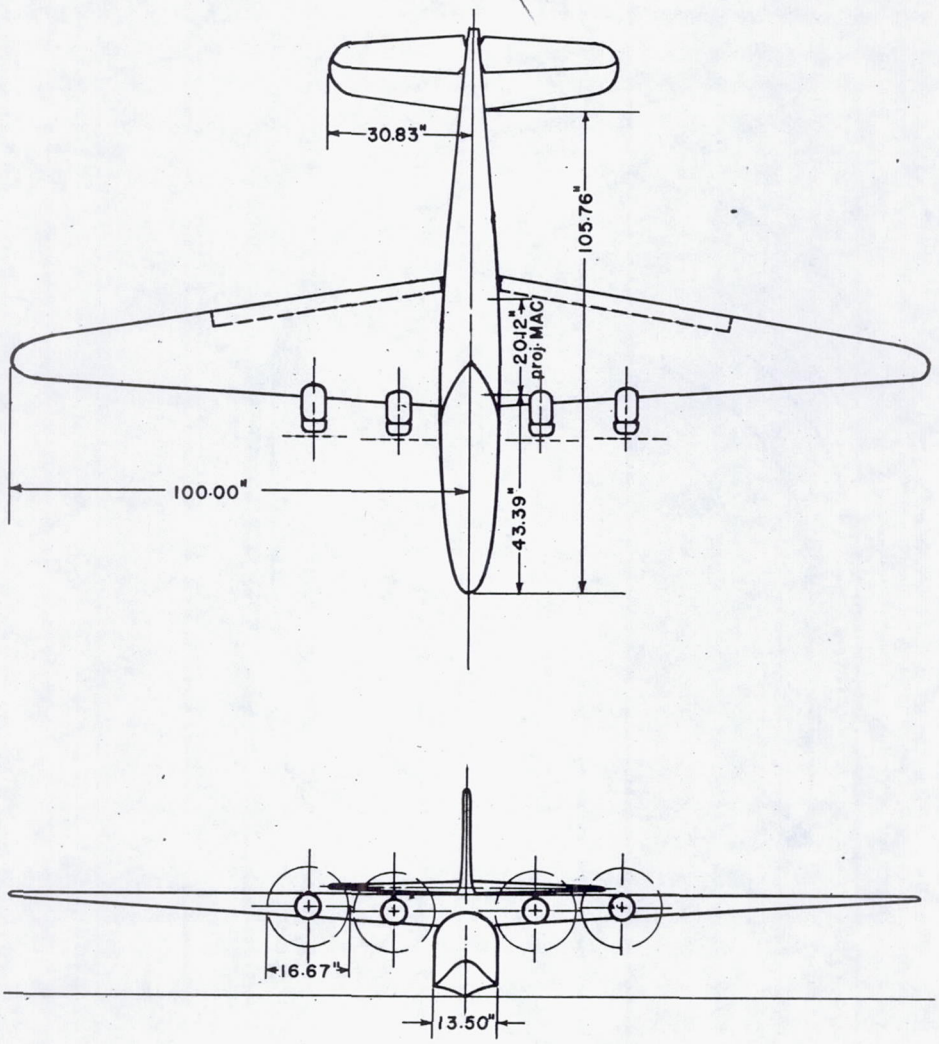
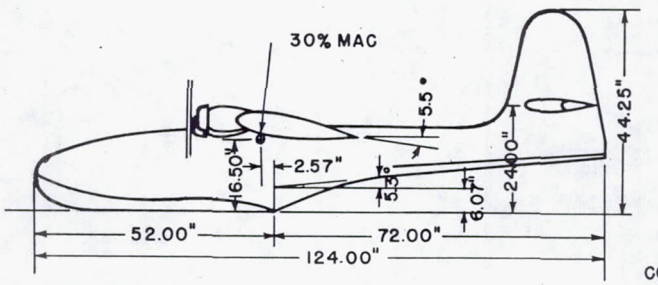


Figure 1.- Photograph of the dynamic model with the low-drag planing-tail hull.

CONFIDENTIAL



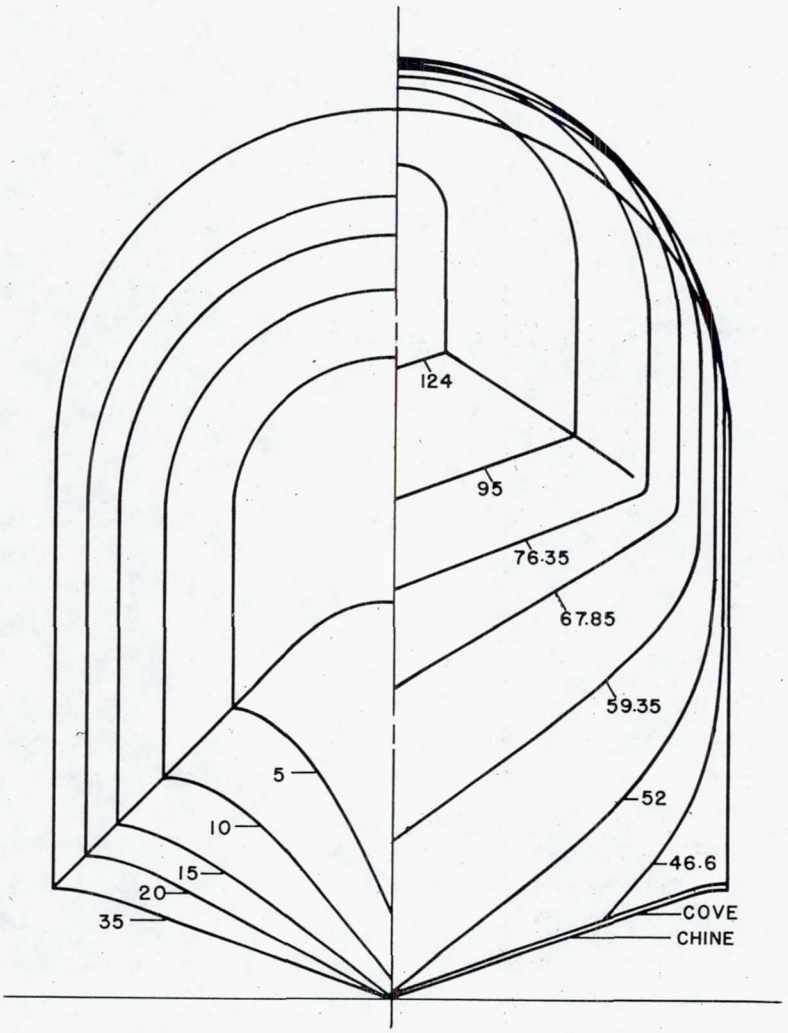


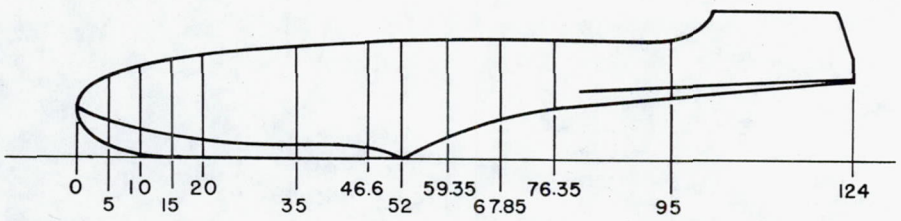
NATIONAL ADVISORY
COMMITTEE FOR AERONAUTICS

Figure 2.-General arrangement of the planing-tail model.

CONFIDENTIAL

CONFIDENTIAL





NATIONAL ADVISORY
COMMITTEE FOR AERONAUTICS

Figure 3.- Planing-tail hull lines.

CONFIDENTIAL

CONFIDENTIAL

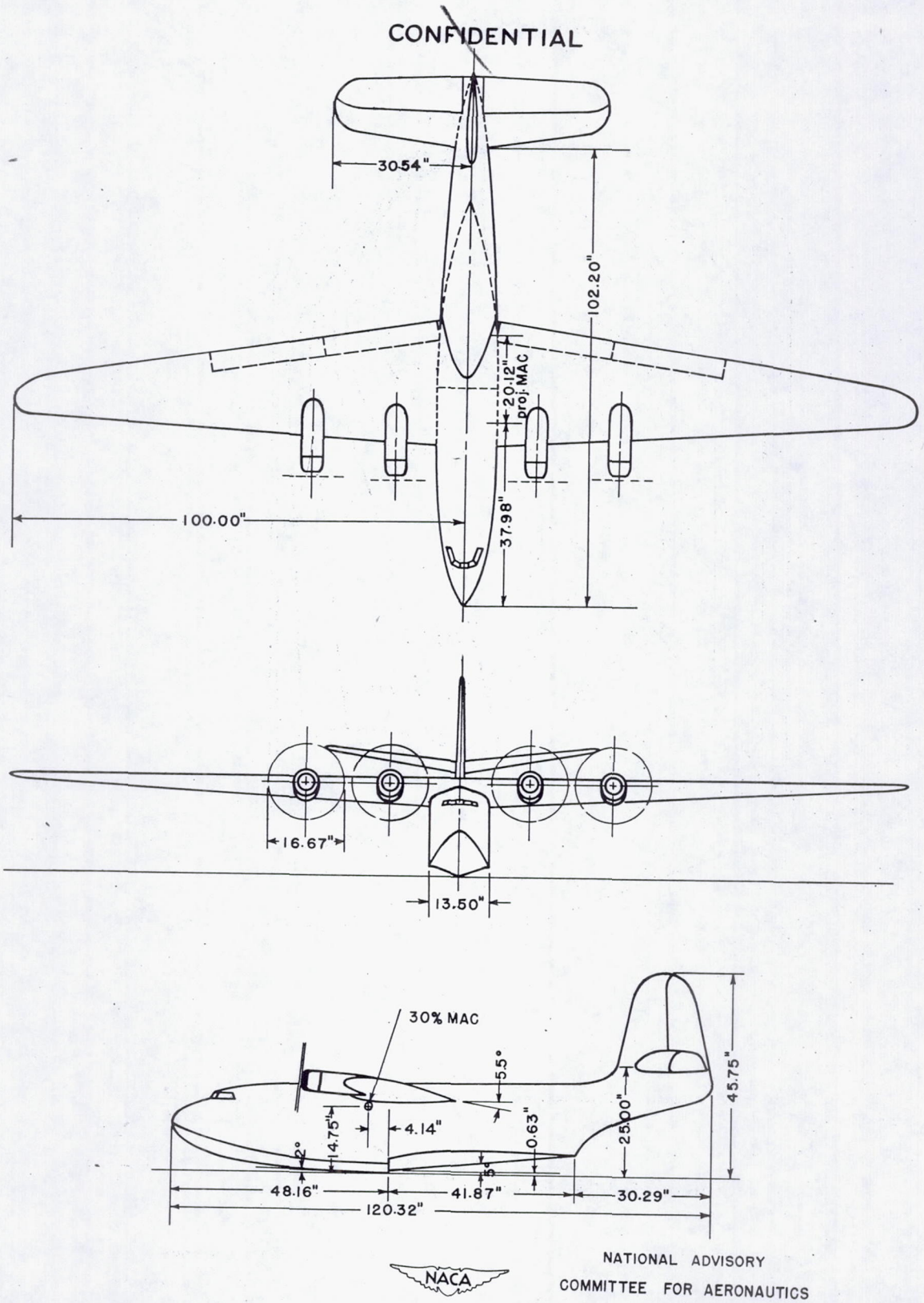
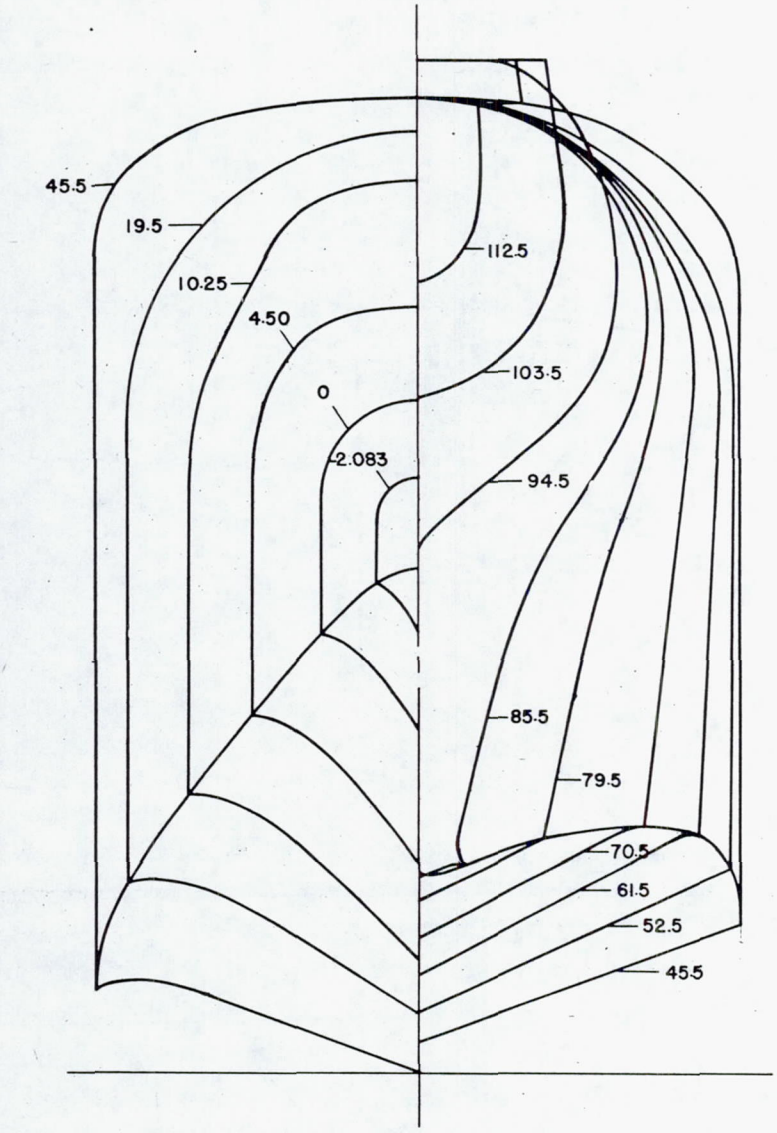
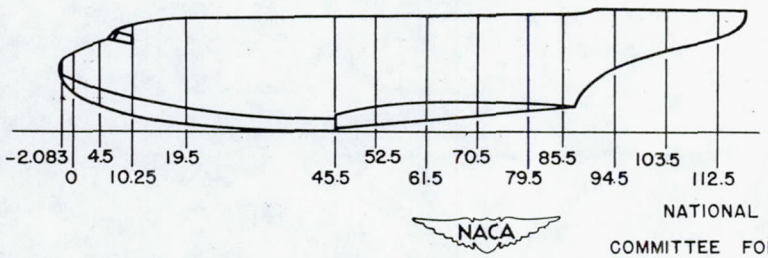


Figure 4.- General arrangement of the conventional-hull model.

CONFIDENTIAL

CONFIDENTIAL





NATIONAL ADVISORY
COMMITTEE FOR AERONAUTICS

Figure 5.--Conventional hull lines.

CONFIDENTIAL

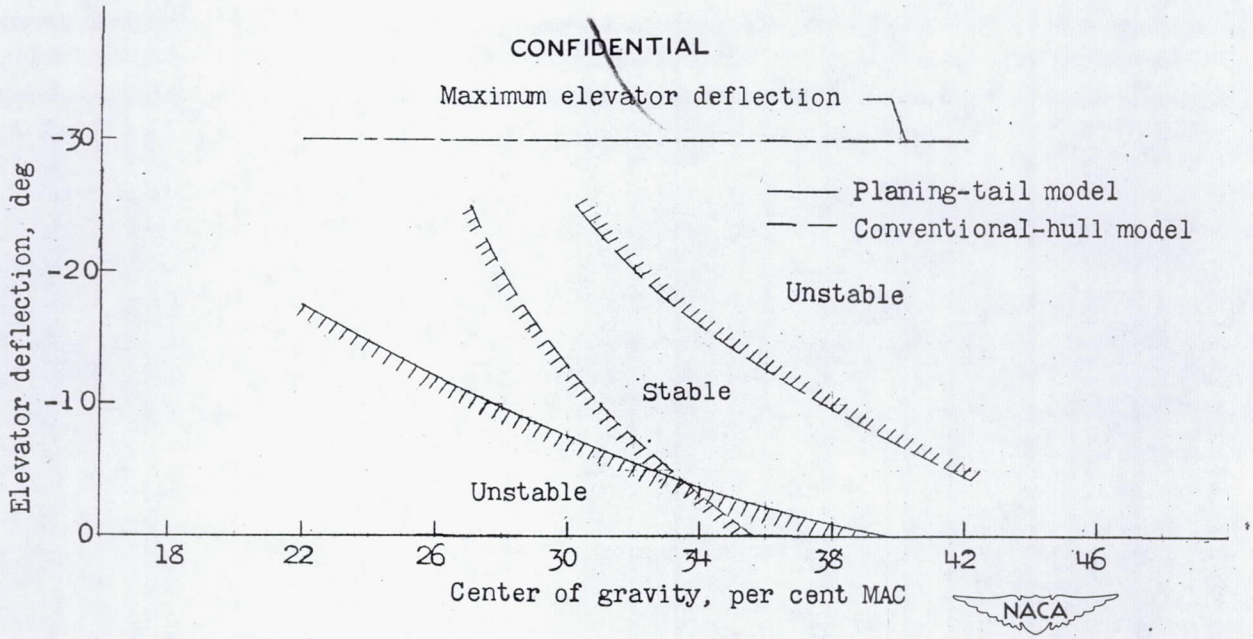


Figure 6.- Center of gravity limits of stability. Gross load coefficient = 0.94, full power.

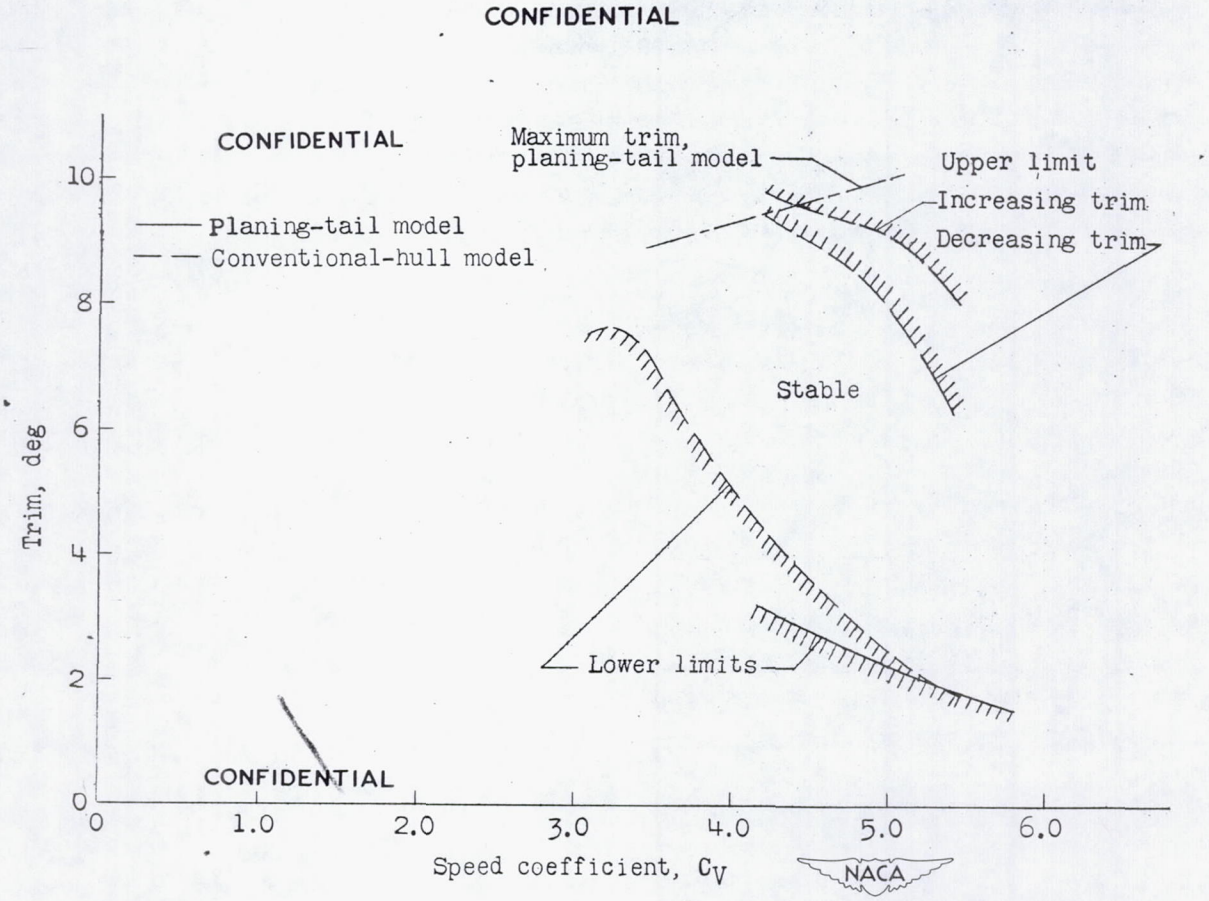


Figure 7.- Trim limits of stability. Gross load coefficient = 0.94, full power.

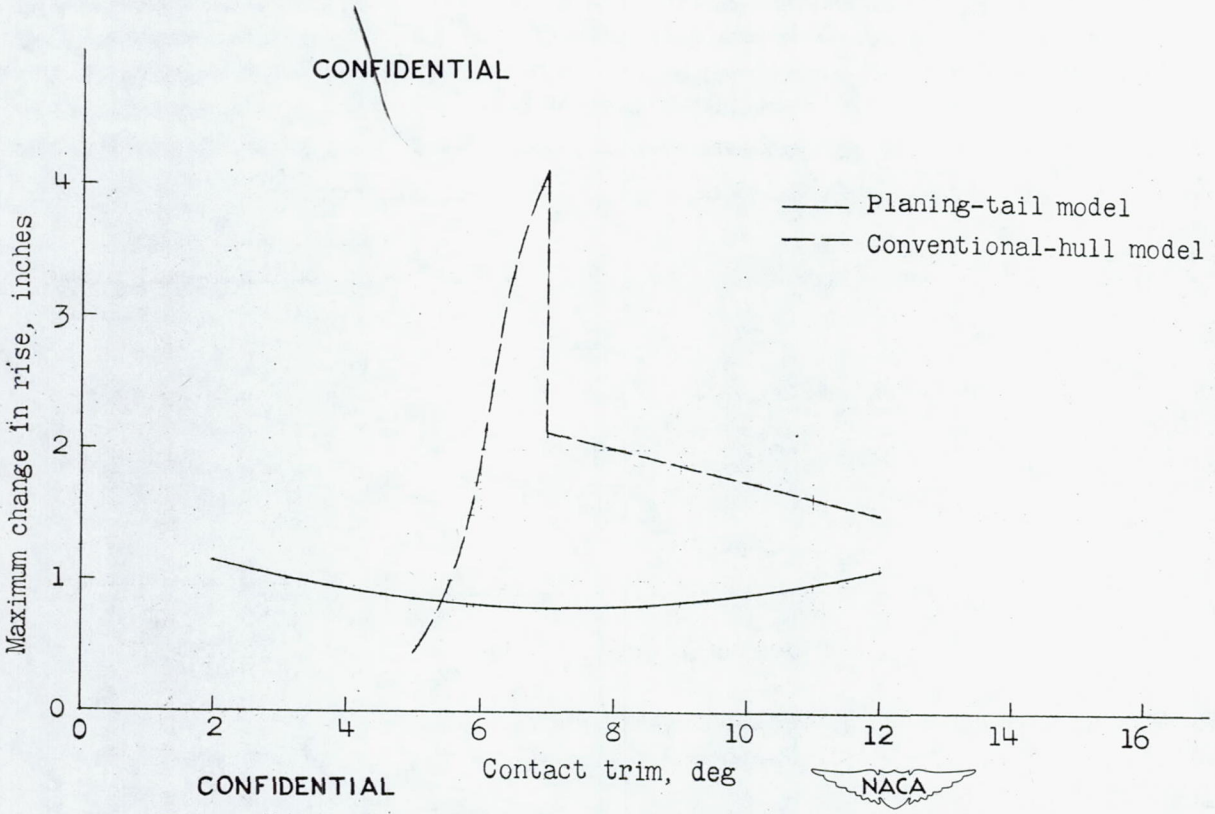


Figure 8.- Landing stability. Gross load coefficient = 0.94, 1/4 full power.

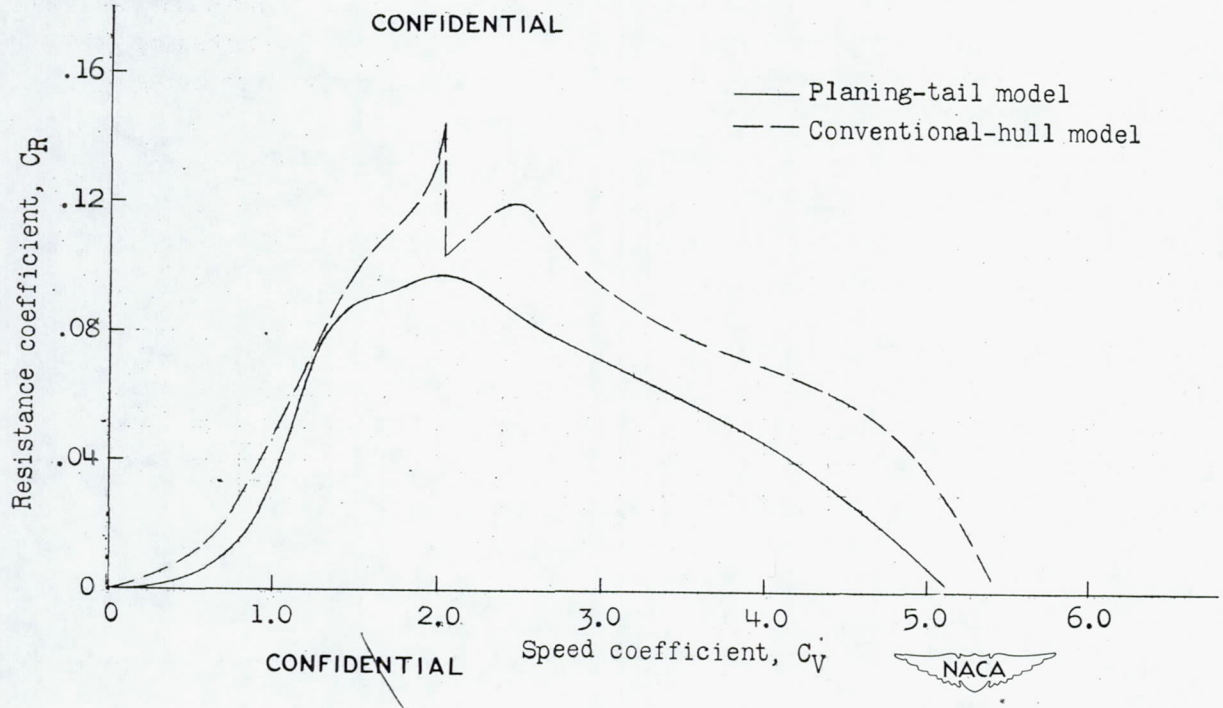


Figure 9.- Resistance. Gross load coefficient = 0.94.

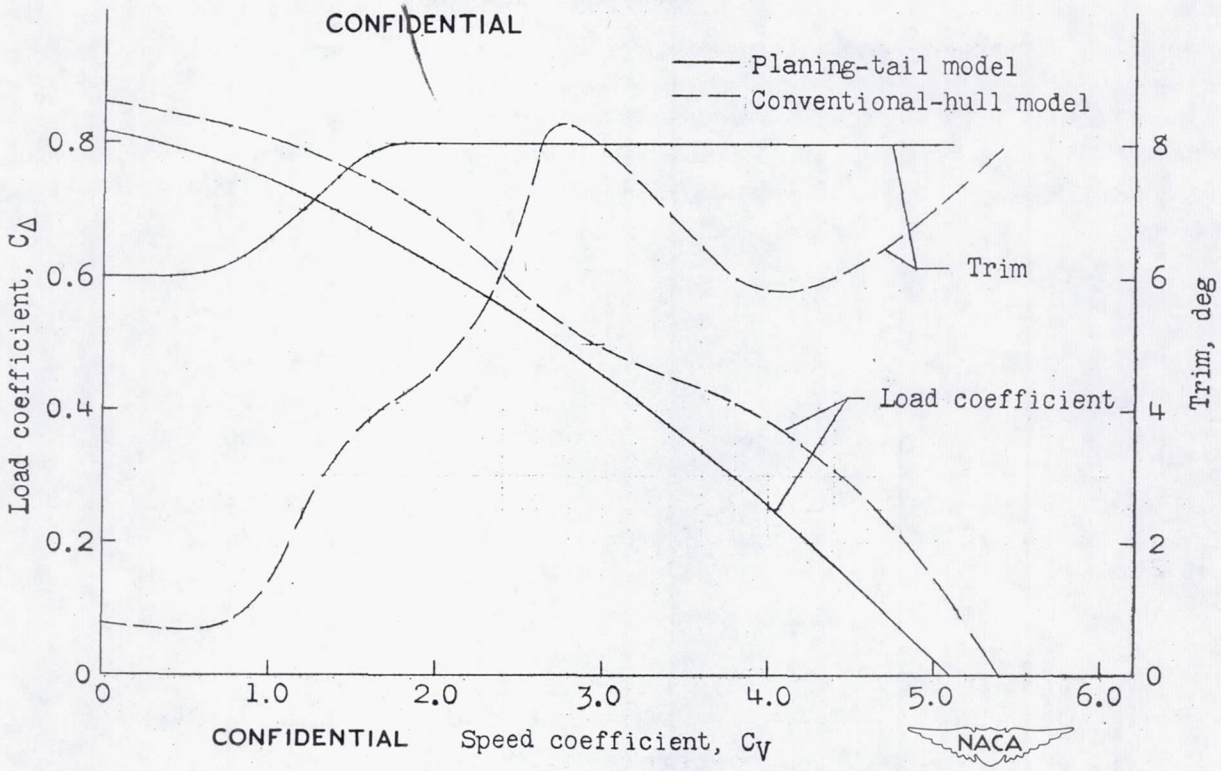


Figure 10.- Variation of trim and load coefficient with speed. Gross load coefficient = 0.94.

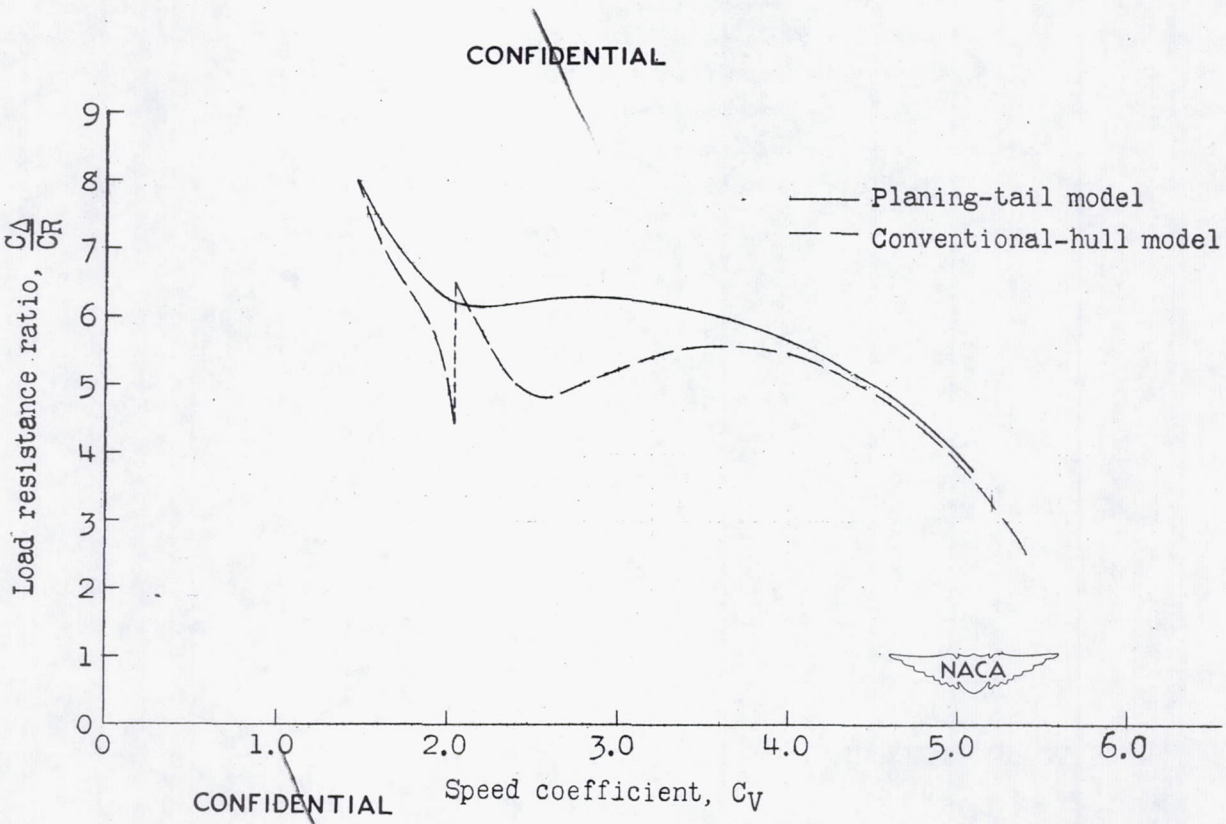


Figure 11.- Variation of load-resistance ratio with speed. Gross load coefficient = 0.94.

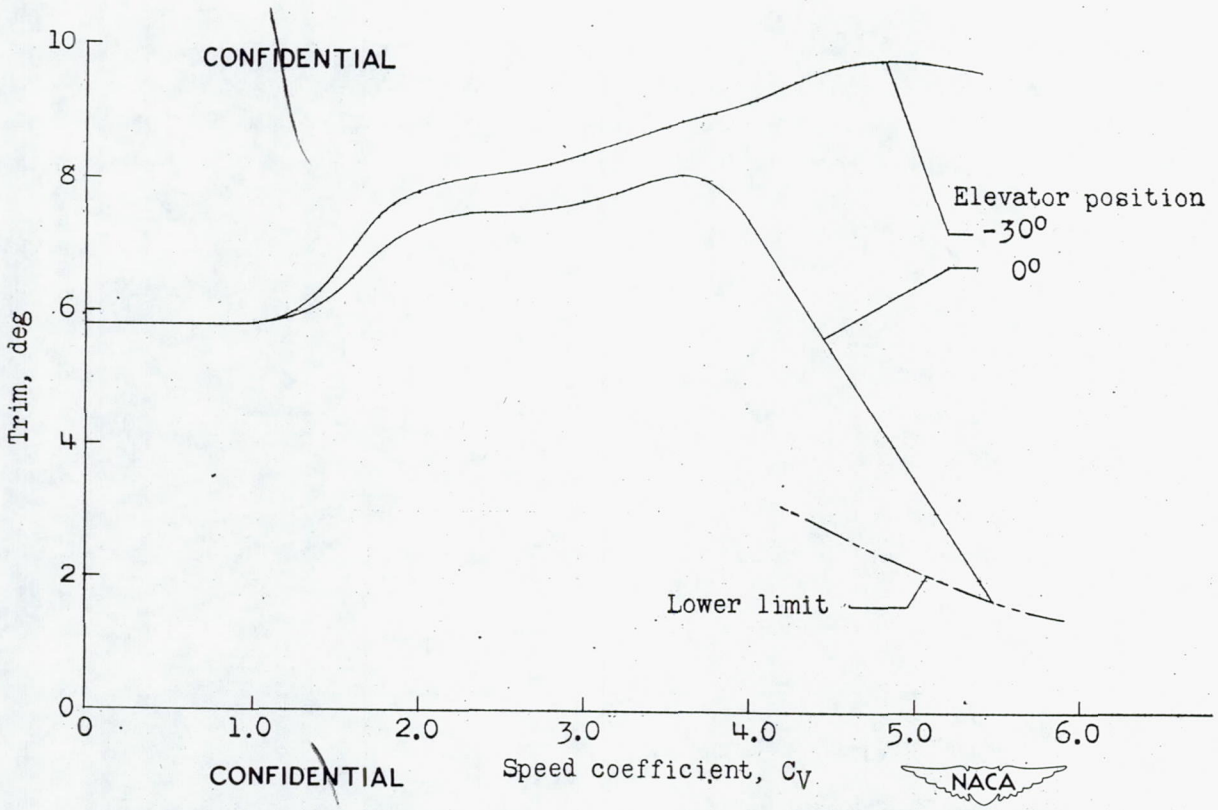


Figure 12.- Variation of trim with speed for planing-tail model. Gross load coefficient = 0.94, center of gravity 30 % MAC, full power.

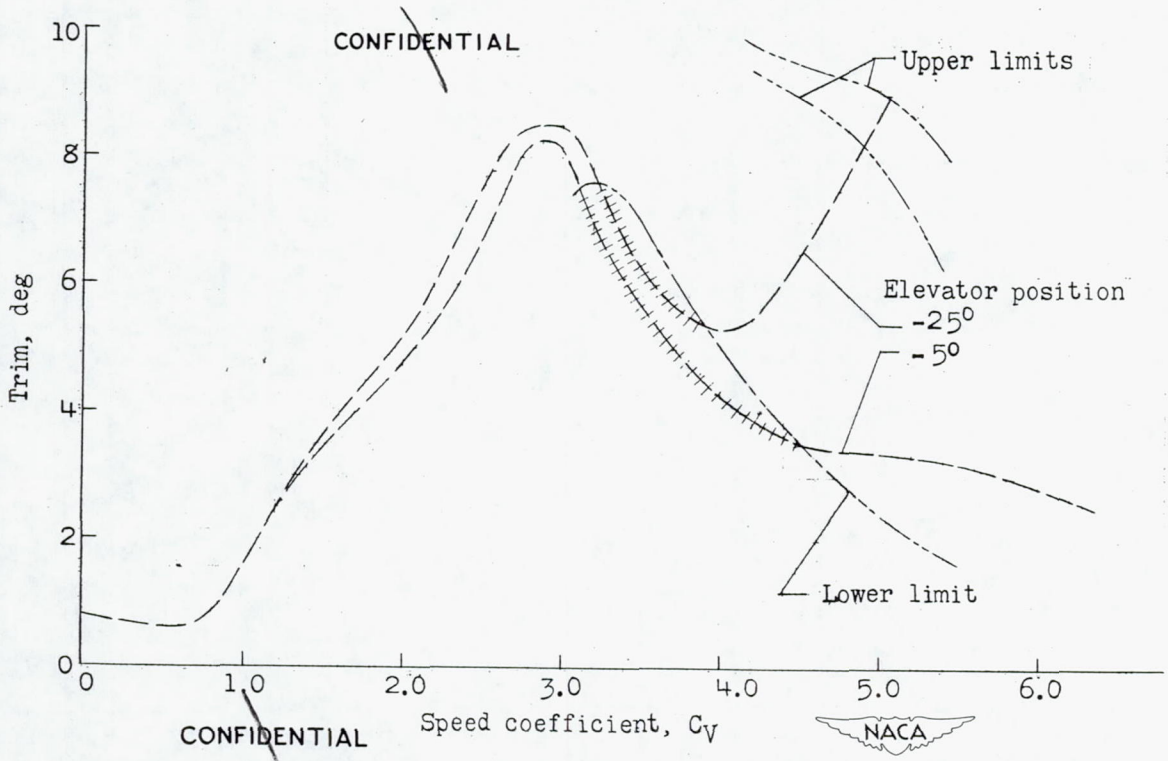
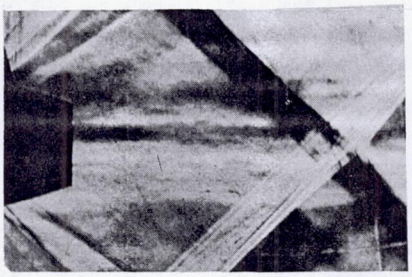
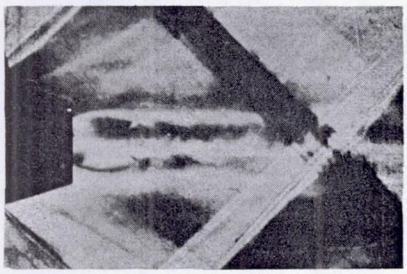


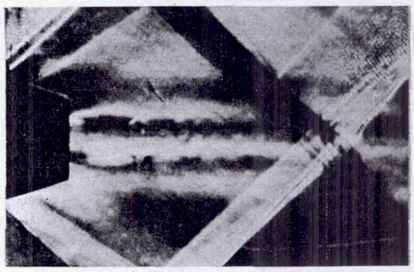
Figure 13.- Variation of trim with speed for conventional-hull model. Gross load coefficient = 0.94, center of gravity 30 % MAC, full power.



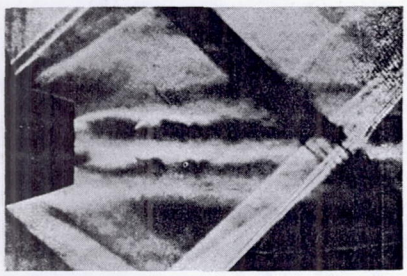
No flow



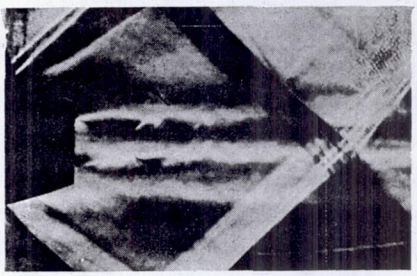
p_j/p_s = 3.10; w = 0



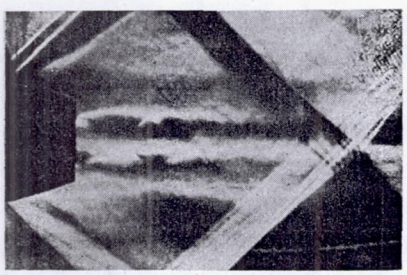
p_j/p_s = 3.10; w = .02



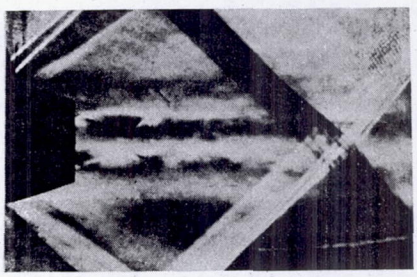
p_j/p_s = 3.10; w = .04



p_j/p_s = 3.10; w = .06



p_j/p_s = 3.10; w = .08



p_j/p_s = 3.10; w = .10

L-85665

Figure 10.- Schlieren photographs for second shroud at M = 1.62 illustrating flow mechanism of sonic nozzle at jet static-pressure ratio of 3.10 together with various secondary mass-flow ratios.

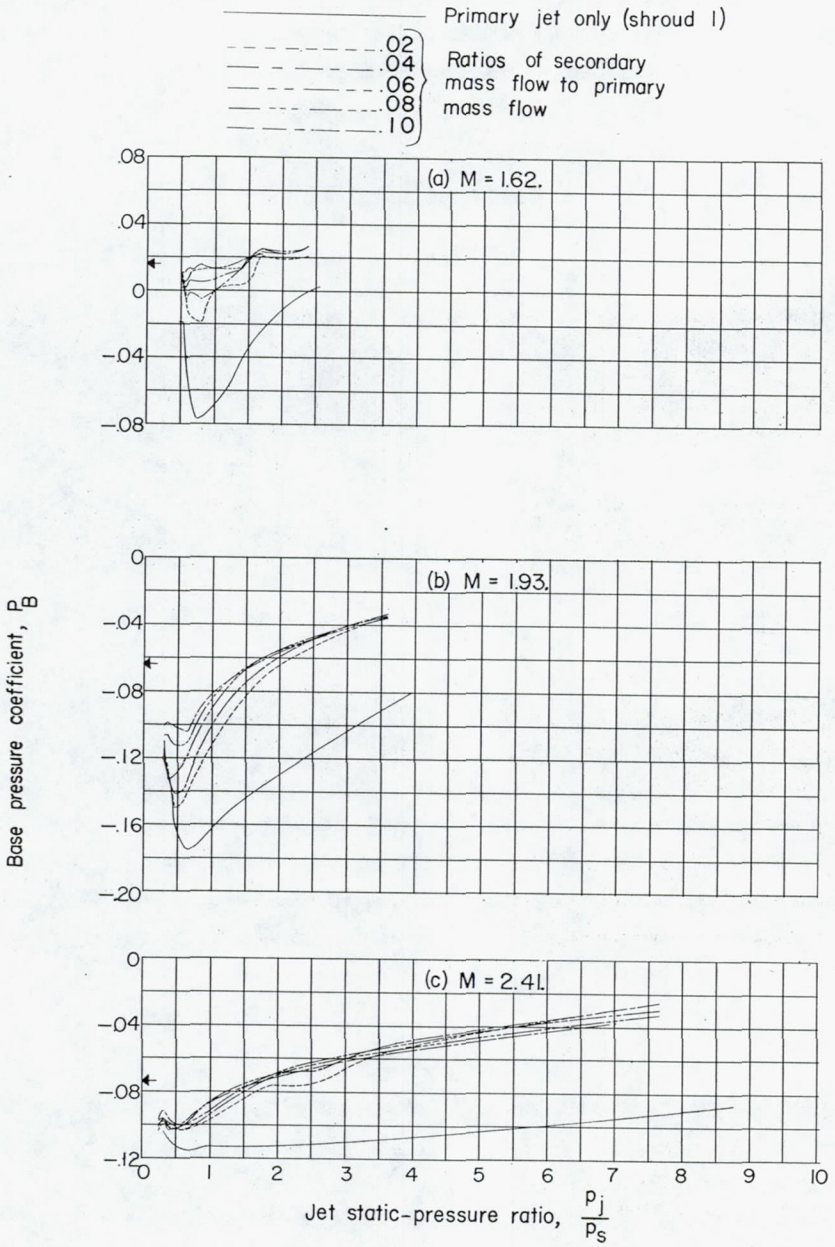
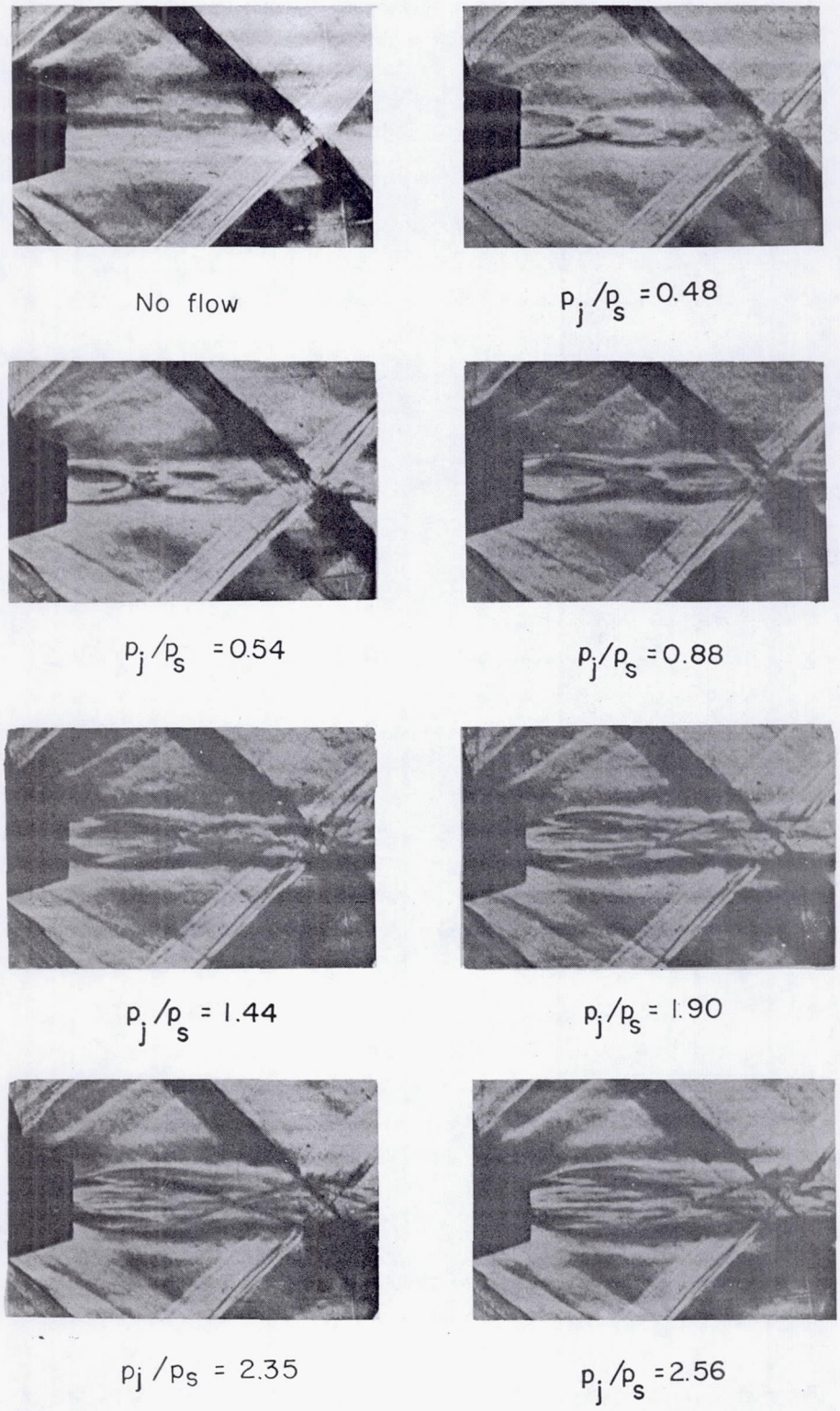


Figure 11.- Variation of base pressure coefficient of first shroud (d/D_B = 0.82) with different values of primary jet pressure ratio and secondary mass-flow ratio. Supersonic nozzle; M = 1.62, 1.93, and 2.41. Arrows indicate base-pressure values for no primary or secondary flow.



L-85666

Figure 12.- Schlieren photographs for first shroud (d/D_B = 0.82) at various jet pressure ratios. Supersonic nozzle; M = 1.62.

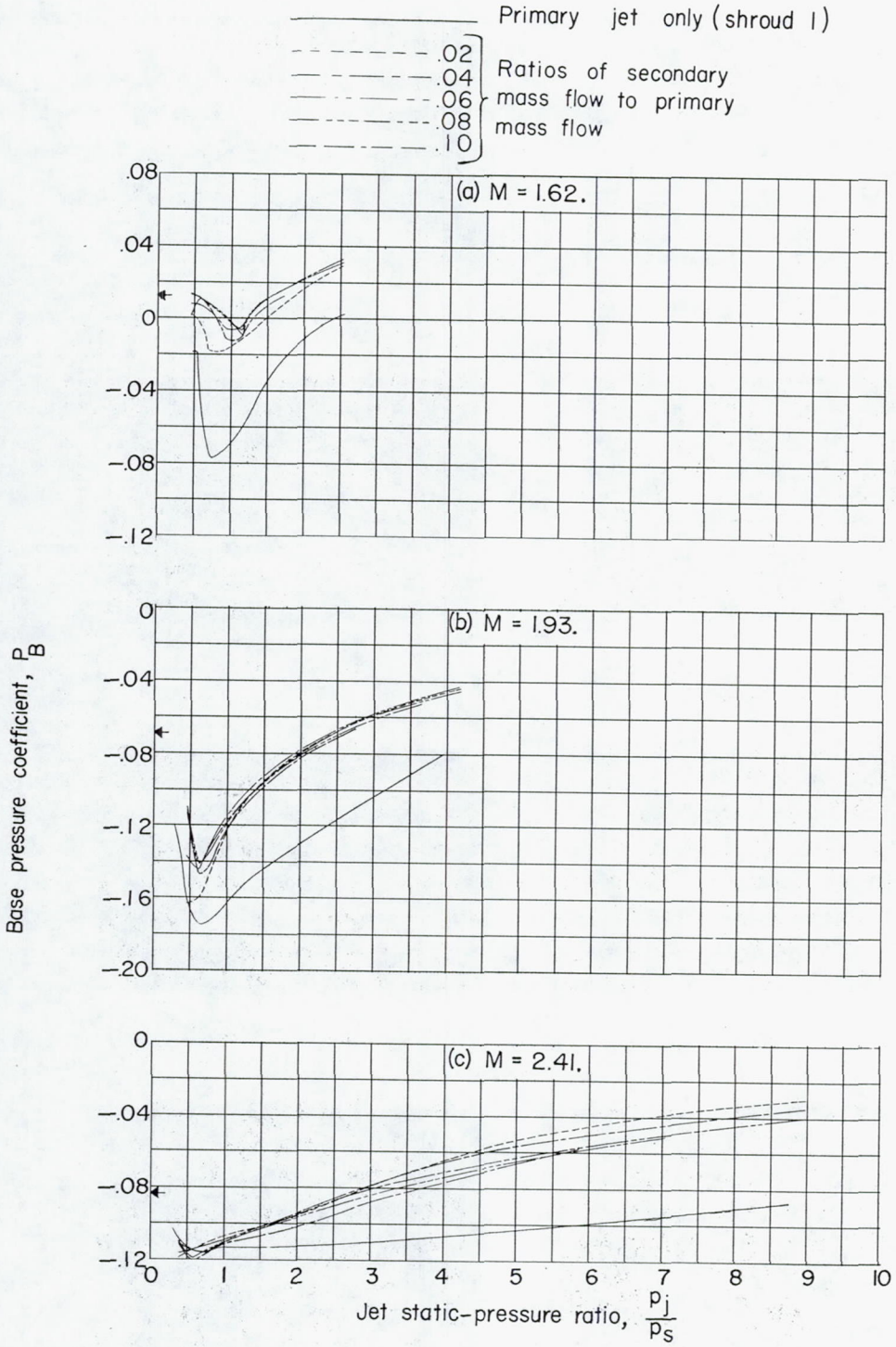
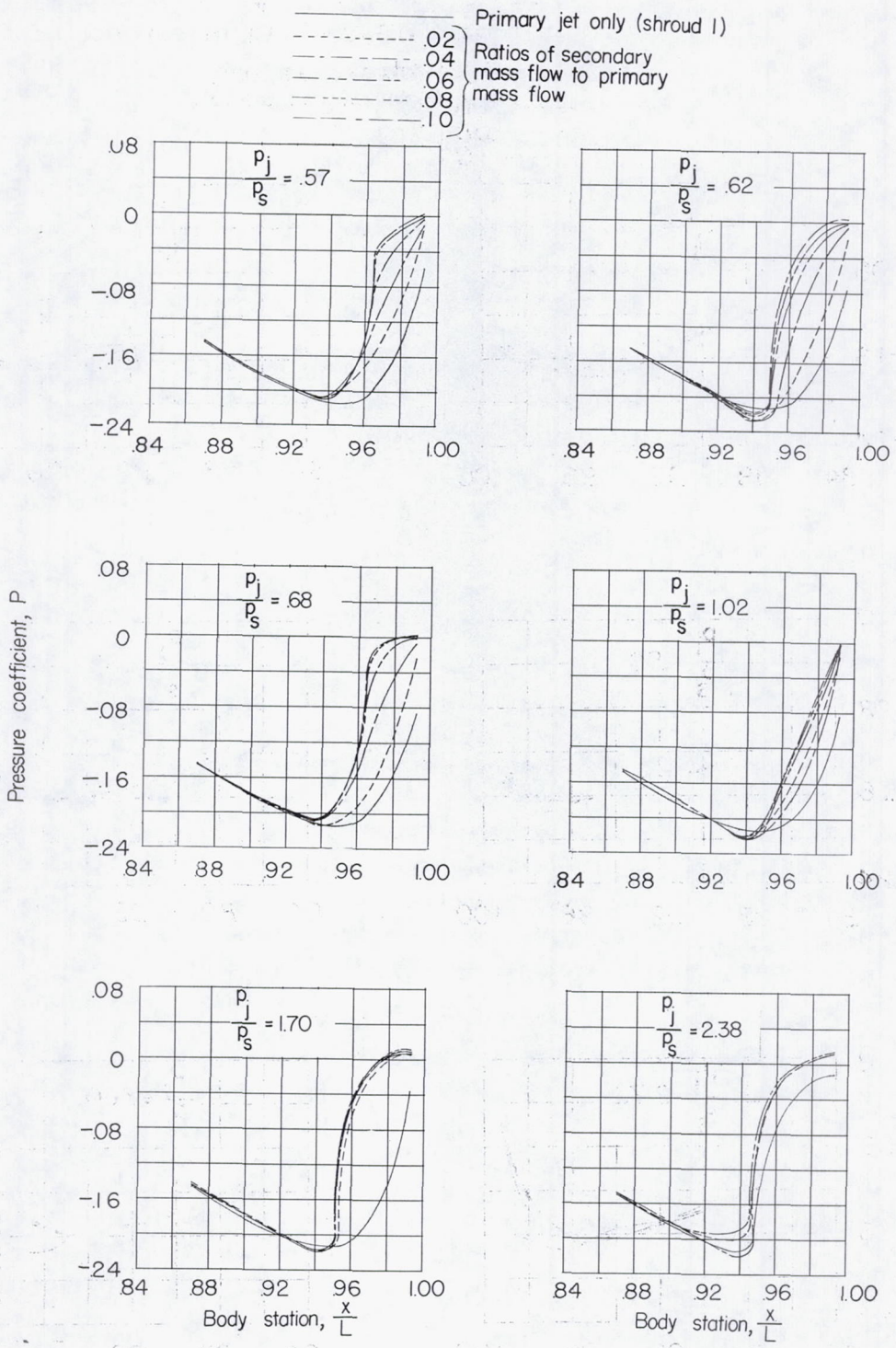
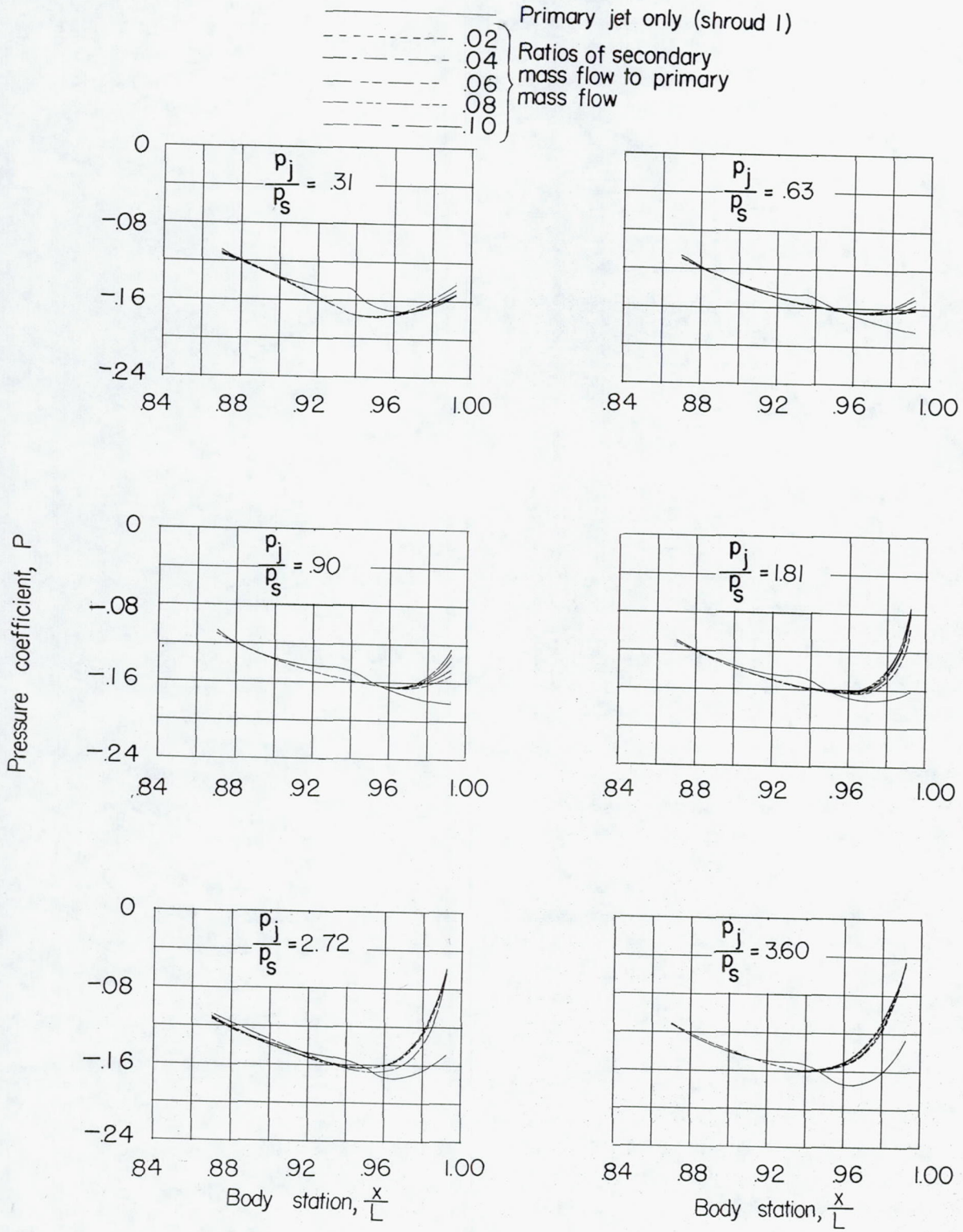


Figure 13.- Variation of base pressure coefficient of second shroud (d/D_B = 0.73) with different values of primary jet pressure ratio and secondary mass-flow ratio. Supersonic nozzle; M = 1.62, 1.93, and 2.41. Arrows indicate base-pressure values for no primary or secondary flow.



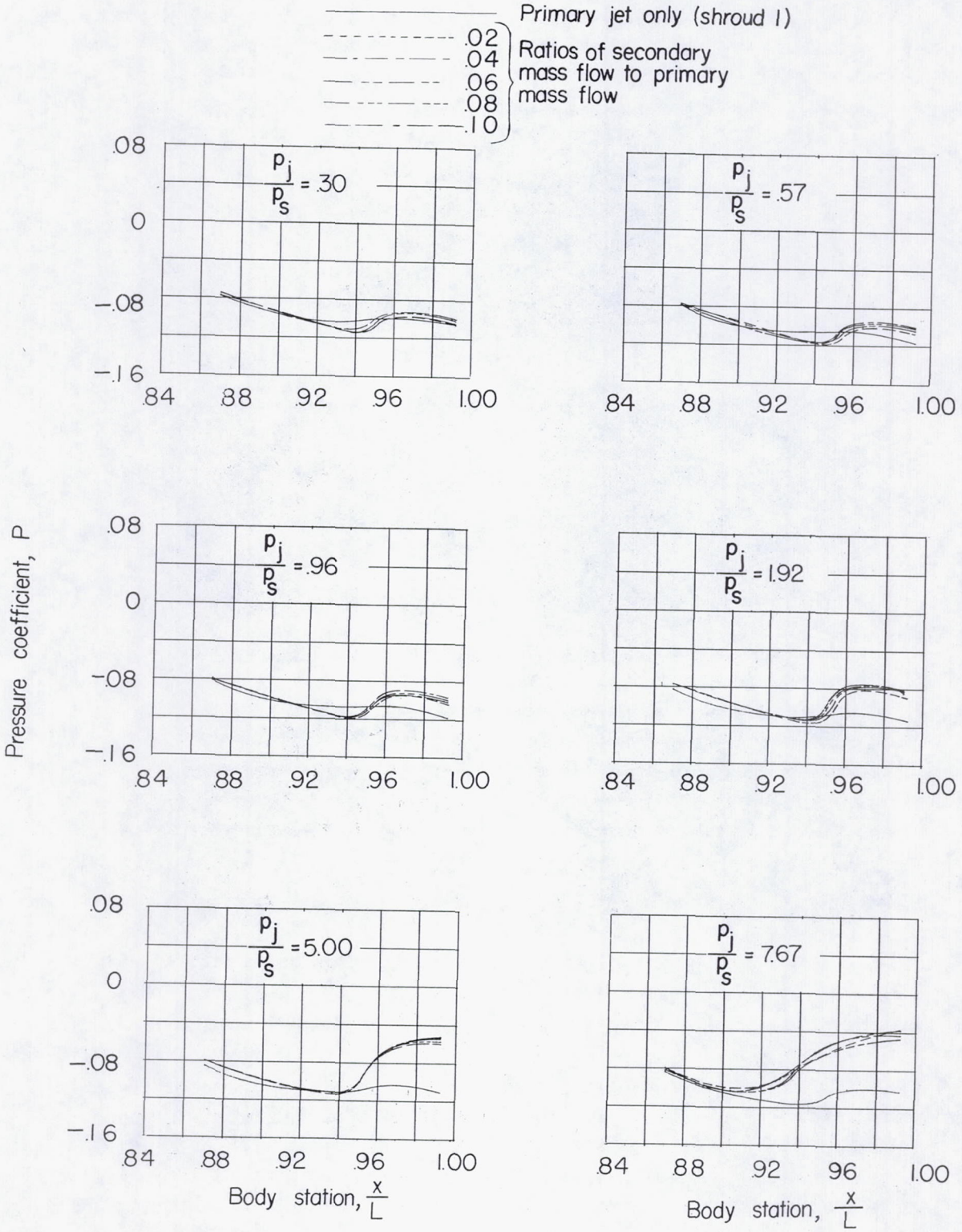
(a) M = 1.62.

Figure 14.- Variation of boattail pressure coefficient on first shroud (d/D_B = 0.82) for different values of primary jet pressure ratio and secondary mass-flow ratio. Supersonic nozzle.



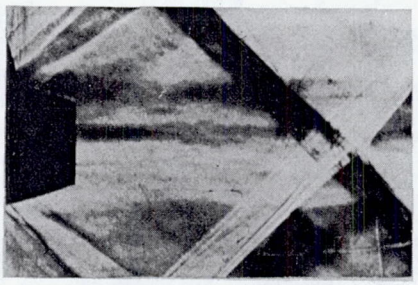
(b) M = 1.93.

Figure 14.- Continued.

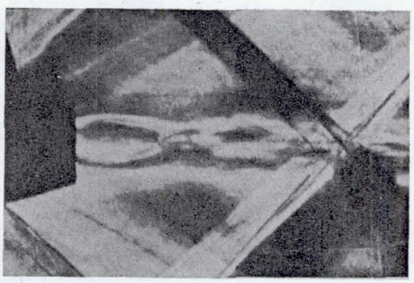


(c) M = 2.41.

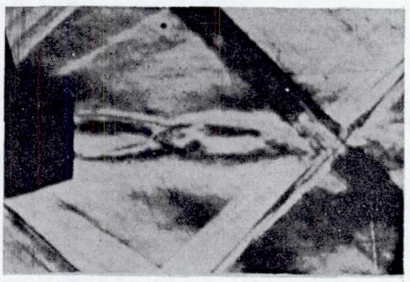
Figure 14.- Concluded.



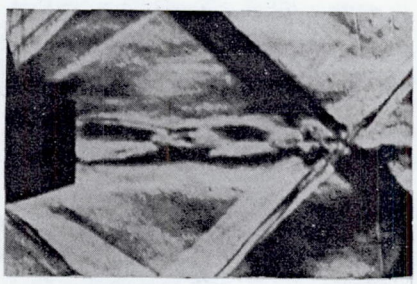
No flow



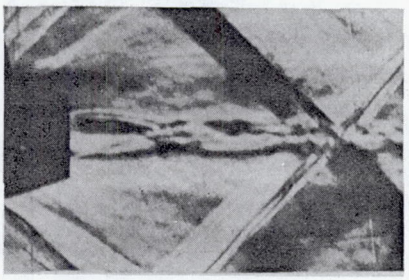
$p_j/p_s = 0.76$; w = 0



$p_j/p_s = 0.68$; w = .02



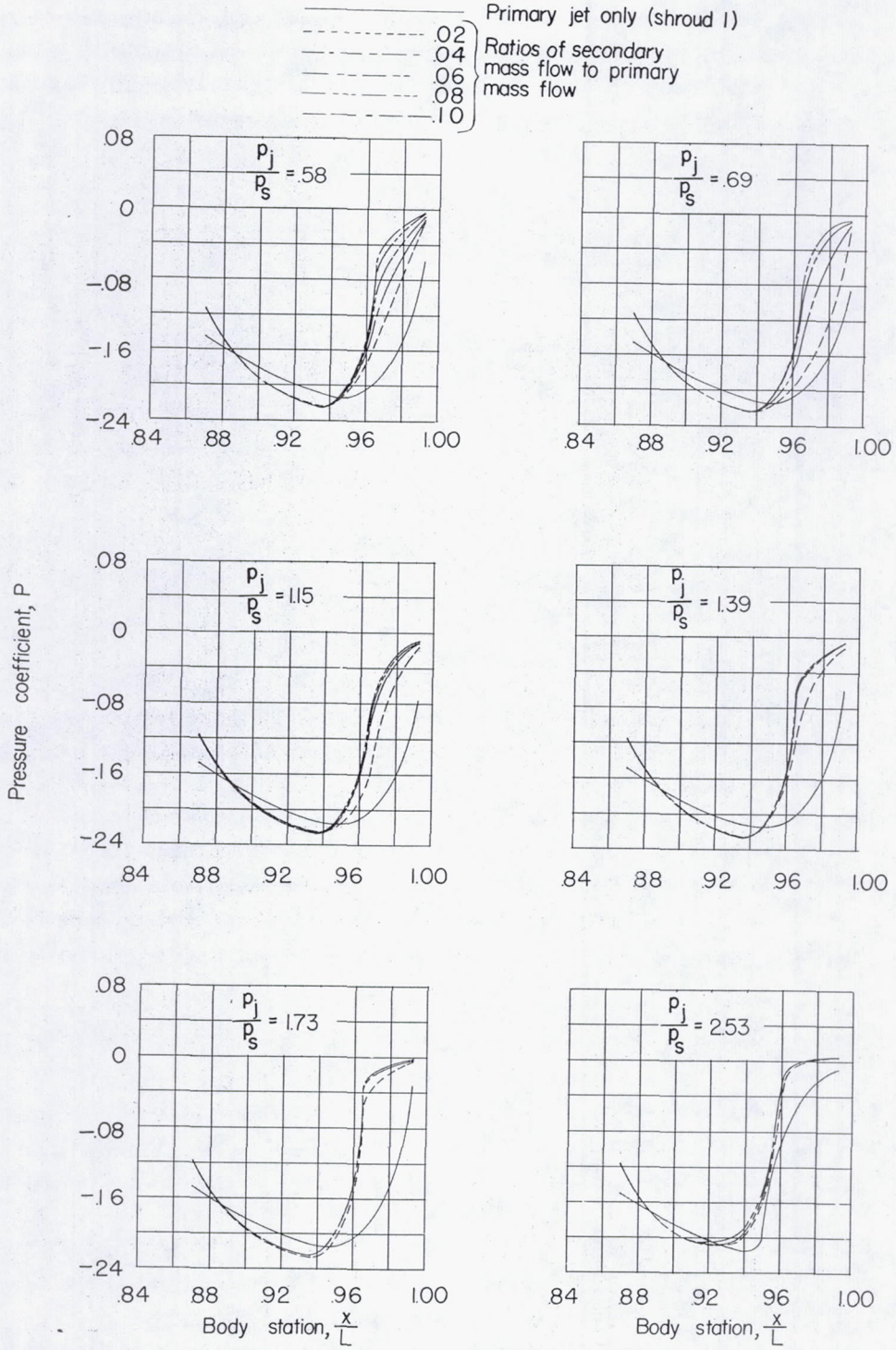
$p_j/p_s = 0.68$; w = .04



$p_j/p_s = 0.68$; w = .06

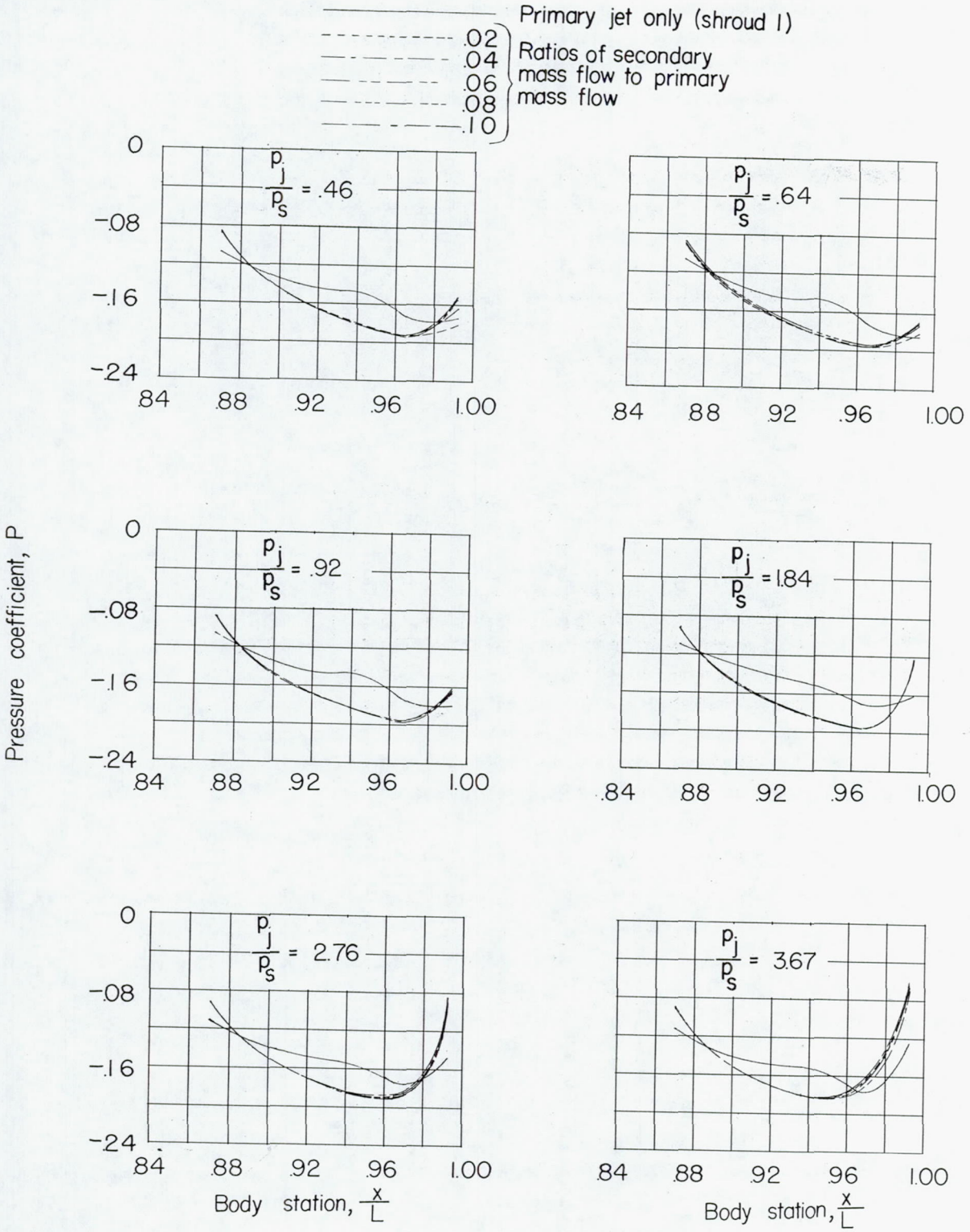
L-85667

Figure 15.- Schlieren photographs for first shroud at M = 1.62 illustrating flow mechanism of supersonic nozzle together with various secondary mass-flow ratios.



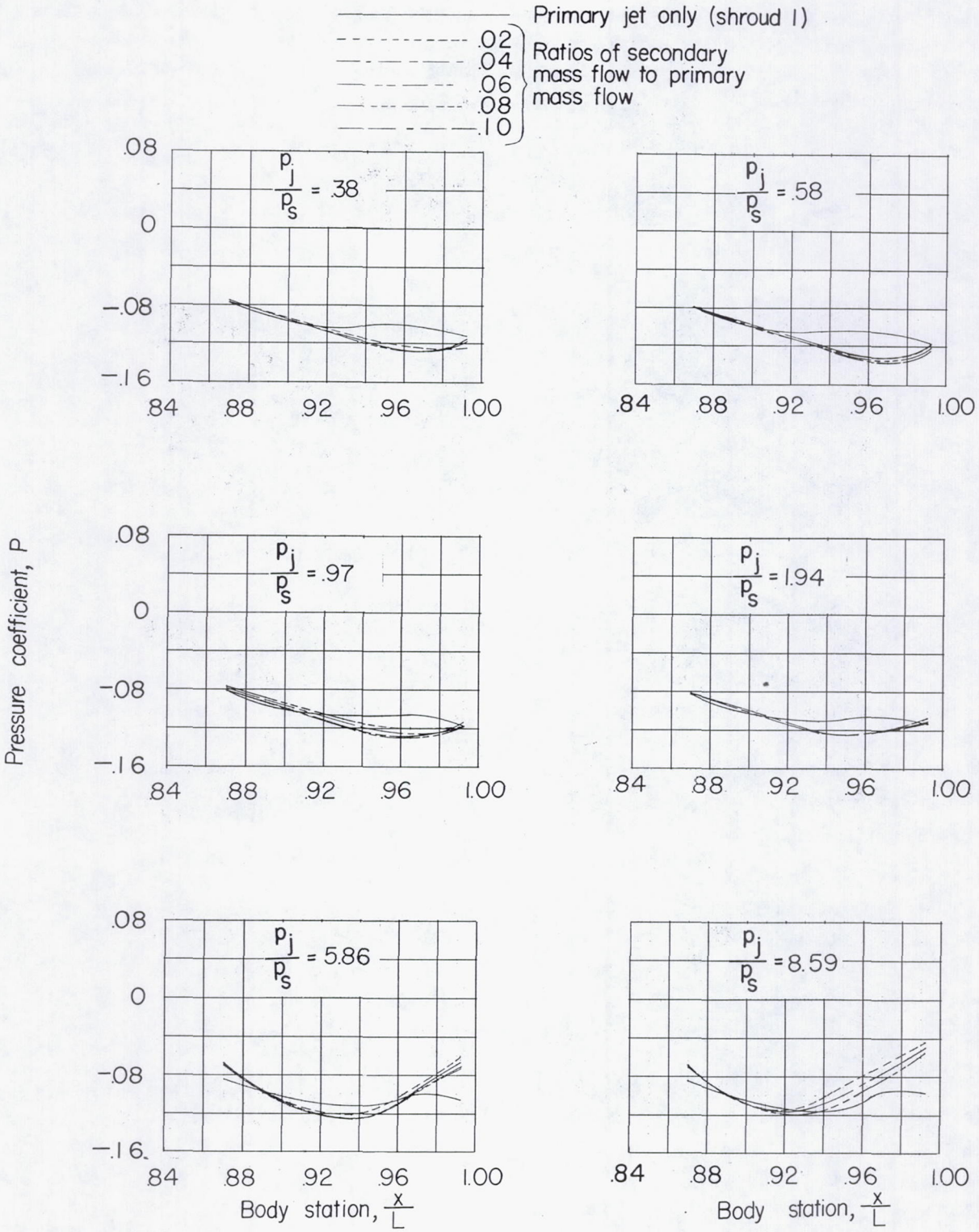
(a) M = 1.62.

Figure 16.- Variation of boattail pressure coefficient on second shroud (d/D_B = 0.73) for different values of primary jet pressure ratio and secondary mass-flow ratio. Supersonic nozzle.



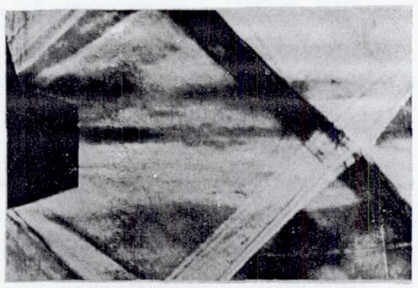
(b) M = 1.93.

Figure 16.- Continued.

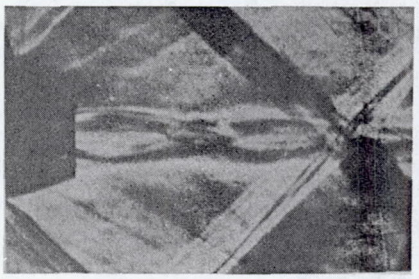


(c) M = 2.41.

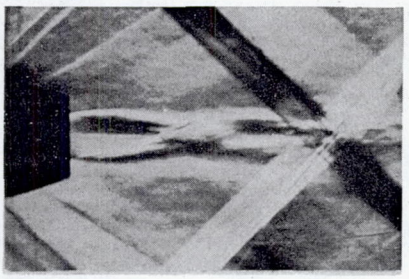
Figure 16.- Concluded.



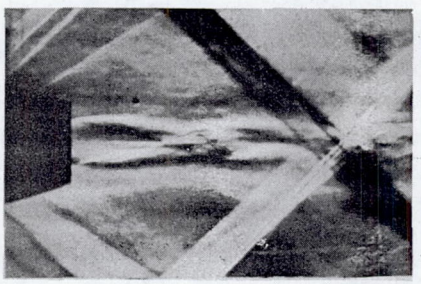
No flow



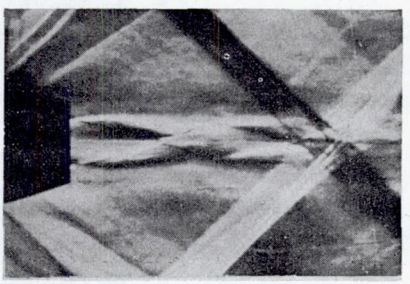
p_j/p_s = 0.88; w = 0



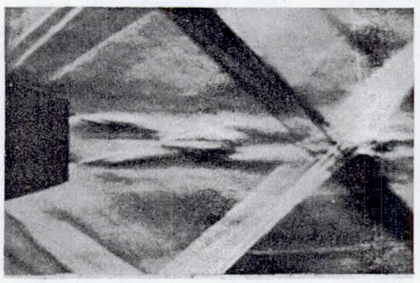
p_j/p_s = 0.92; w = .02



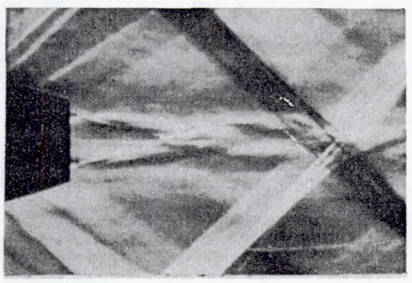
p_j/p_s = 0.92; w = .04



p_j/p_s = 0.92; w = .06



p_j/p_s = 0.92; w = .08



p_j/p_s = 0.92; w = .10

L-85668

Figure 17.- Schlieren photographs for second shroud at M = 1.62 illustrating flow mechanism of supersonic nozzle together with various secondary mass-flow ratios.

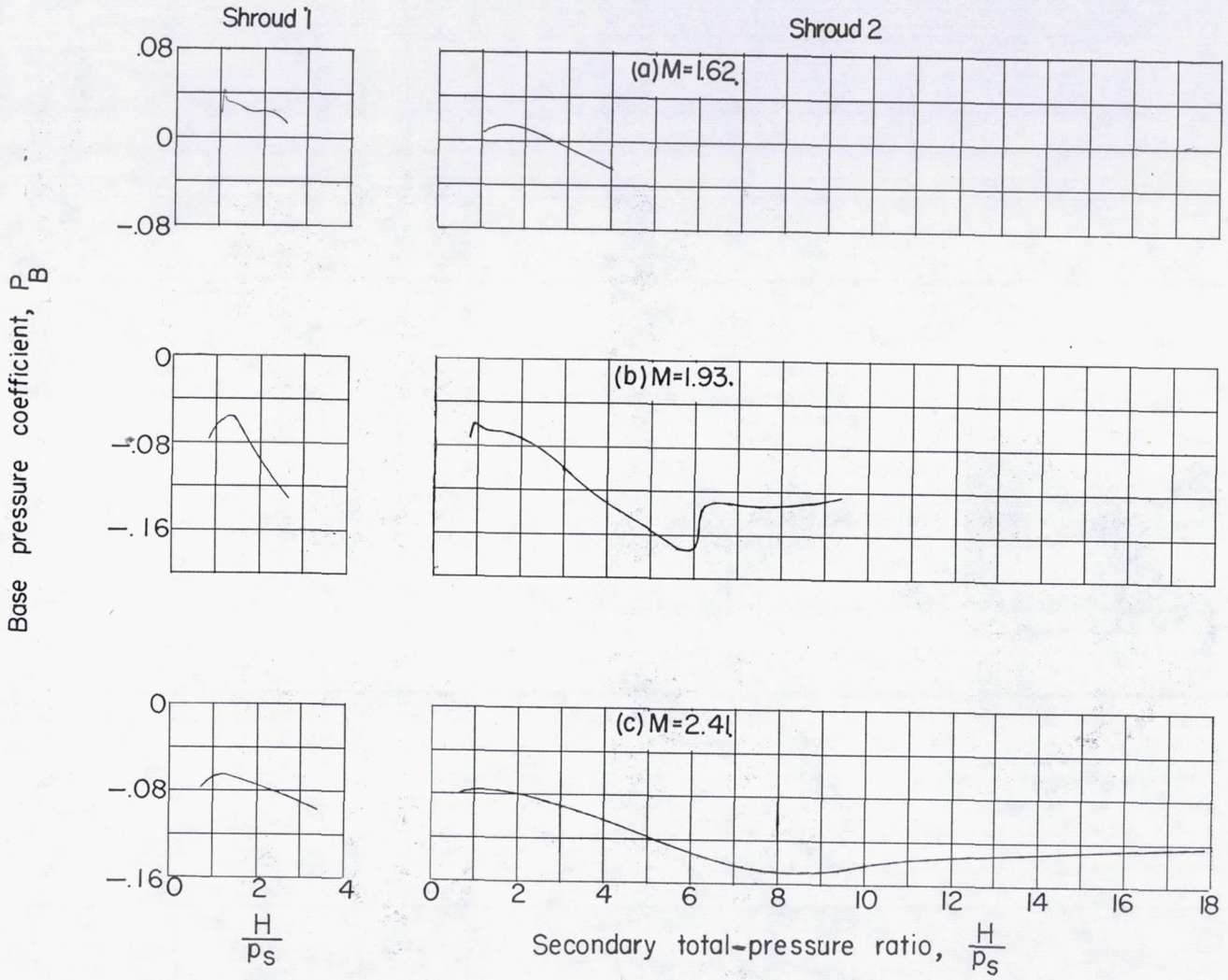
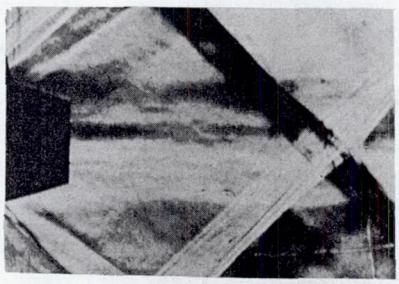
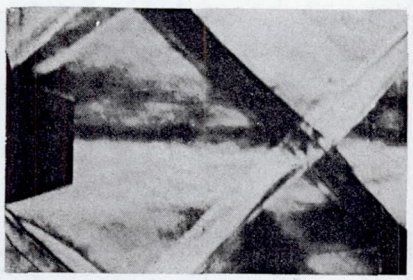


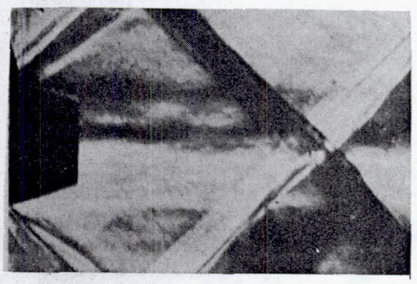
Figure 18.- Variation of base pressure coefficient of both shrouds with different values of secondary total-pressure ratio at free-stream Mach numbers of 1.62, 1.93, and 2.41.



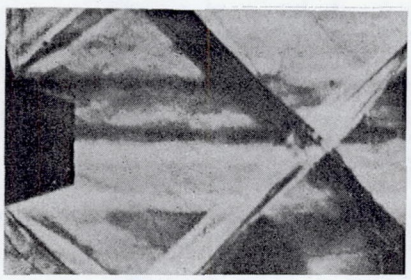
No flow



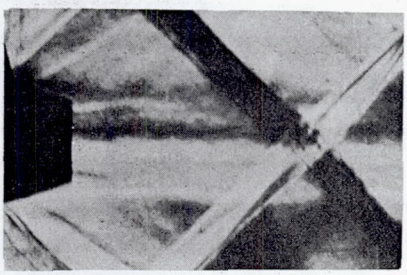
H/p_s =1.04



H/p_s =1.07



H/p_s =1.61



H/p_s =2.50

L-85669

Figure 19.- Schlieren photographs at M = 1.62 for first shroud at various secondary total-pressure ratios.

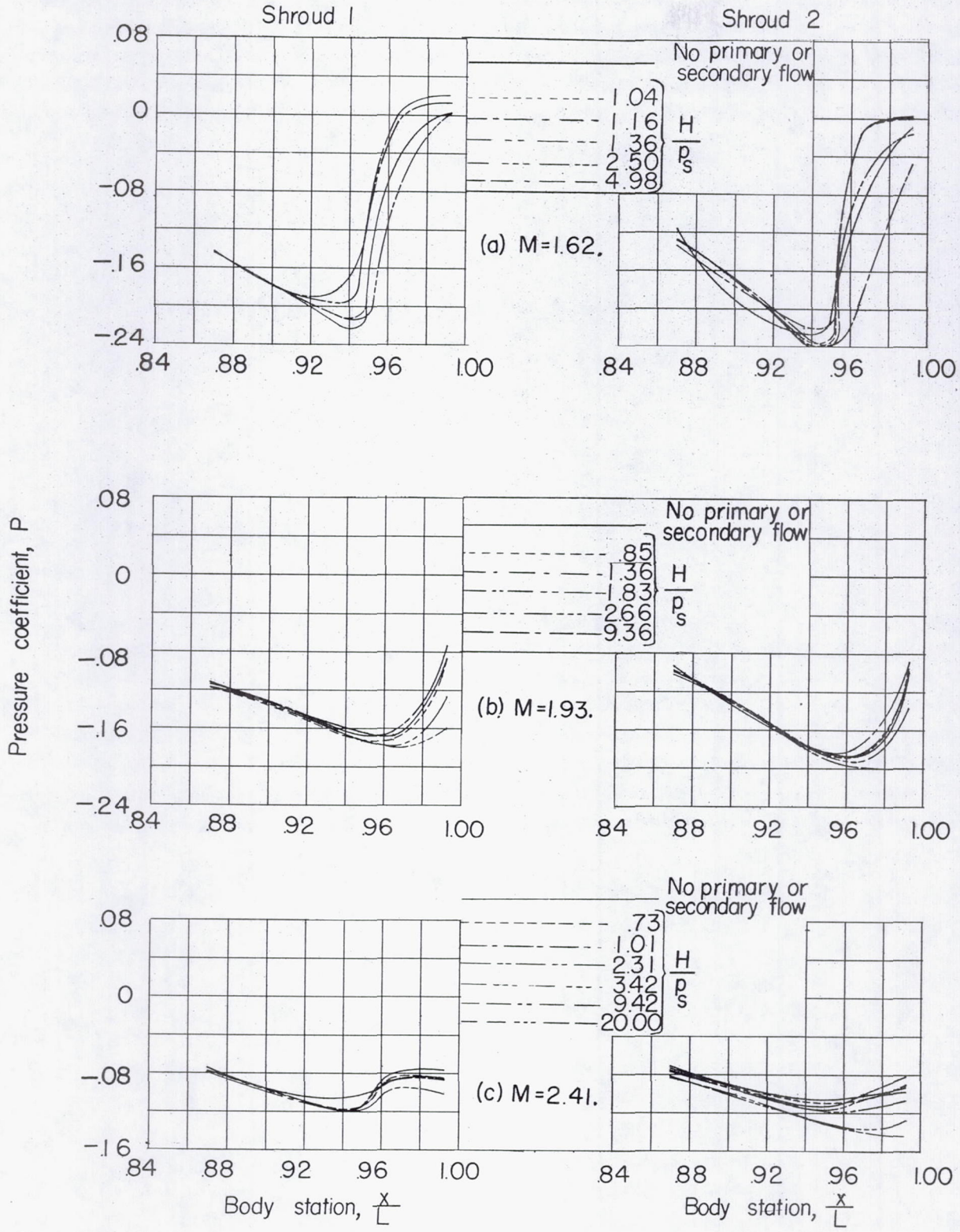


Figure 20.- Effects of secondary mass flow on pressure distributions of both shrouds at M = 1.62, 1.93, and 2.41.